Volume 5 • Number 4 • October 2011
ISSN: 1557-7244

Journal of

APPLIED PACKAGING RESEARCH

Aim and Scope

The *Journal of Applied Packaging Research* is an international forum for the dissemination of research papers, review articles, tutorials and news about innovative or emerging technologies for the packaging industry. The journal is targeted towards the broad packaging community including packaging scientists and engineers in industry or academic research and development, food scientists and technologists, materials scientists, mechanical engineers, industrial and systems engineers, toxicologists, analytical chemists, environmental scientists, regulatory officers, and other professionals who are concerned with advances in the development and applications of packaging.

JOURNAL OF APPLIED PACKAGING RESEARCH—Published quarterly—January, April, July and October by DEStech Publications, Inc., 439 North Duke Street, Lancaster, PA 17602-4967.

This journal is recommended by The National Institute of Packaging Handling and Logistics Engineers (www.niphle.org).

Indexed by Chemical Abstracts Service.

Indexed and abstracted by Pira International.

Subscriptions: Annual $319 (Print), $319 (Electronic) and $344 (Print and Electronic). Single copy price $95.00. Foreign subscriptions add $45 per year for postage.

(ISSN 1557-7244)

DEStech Publications, Inc.
439 North Duke Street, Lancaster, PA 17602-4967, U.S.A.

CONTENTS

Research

Shock Response of a Frictional-viscous Damping Model of Cushioning Material

CHEN ZHONG[1], KATSUHIKO SAITO[2,*] and KAZUAKI KAWAGUCHI[3]

[1]*Ph.D. Candidate, Kobe University, Fukaeminami, Higashinada, Kobe, Japan*
[2]*Professor, Ph.D. in Engineering, Transport Packaging Laboratory, Kobe University, Fukaeminami, Higashinada, Kobe, Japan*
[3]*Ph.D. in Engineering, Shinyei Technology Co., LTD., Japan*

ABSTRACT: The shock response curve is like a half-sine pulse for quasi-linear cushioning materials and like a trapezoidal pulse for structural cushioning materials (SCM). The conventional viscous damping model can explain the experimental results for quasi-linear cushioning materials but not completely explain the results for SCM. Therefore, a new physical model that considers both friction and viscous damping was proposed. To verify this model, a half-sine wave as the input acceleration pulse was used and mathematical simulations were performed. Next, a mathematical equation for the shock response of this model was deduced. Finally, both models were compared with the experimental data and the results showed that our model describes the shock response of SCM more accurately.

INTRODUCTION

MANY distribution hazards affect products during transportation. One such hazard is shock. For shock hazards, the shock response curve is an essential indicator of the cushioning performance of the cushioning material.

Based on previous research [1], the shock response curve for a quasi-linear cushioning material such as expanded polyethylene (EPE) [Figure 1(a)] is curve C1 in Figure 1(b). This curve is smooth and similar to a half-sine pulse. On the other hand, the shock response curve for a structural cushioning material (SCM) such as a sleeve composed of corrugated fiberboard [Figure 2(a)] is curve C3 in Figure 2(b). This curve is a trapezoidal pulse with no prominent peaks.

*Author to whom correspondence should be addressed. Email: ksaito@maritime.kobe-u.ac.jp

1557-7244/11/04 197-18

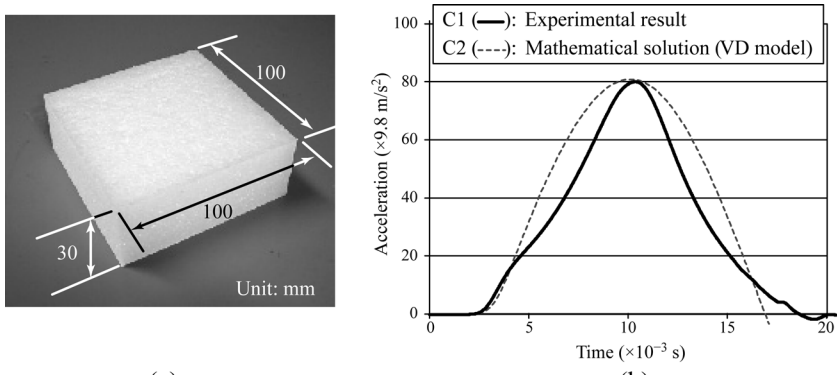

Figure 1. *Expanded polyethylene (EPE) and its shock response curves. (a) EPE; (b) Comparison of EPE shock response curves between experiment and mathematical solution.*

In general, cushioning materials are assumed to follow the viscous damping (VD) model shown in Figure 3. The mathematical shock response curve of EPE is calculated using the VD model, and it is curve C2 in Figure 1(b) [2]. Figure 1(b) shows that the peak acceleration and the impact duration of the theoretical curve basically agree with those of the experimental curve. Therefore, the VD model is applicable for a quasi-linear cushioning material.

If the VD model is used, the mathematical shock response curve of SCM changes to curve C4 in Figure 2(b). Figure 2(b) shows that the peak acceleration and impact duration of the theoretical curve do not match those of the experimental curve. Therefore, the VD model is not

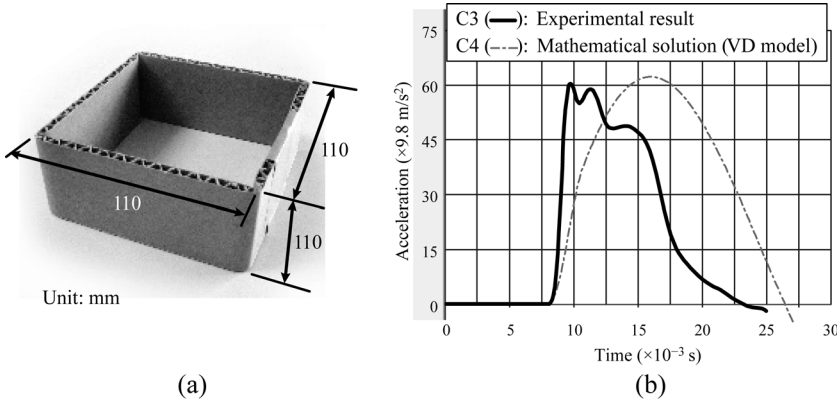

Figure 2. *Test material: sleeve and its shock response curves. (a) Sleeve; (b) Comparison of sleeve shock response curves between experiment and mathematical solution.*

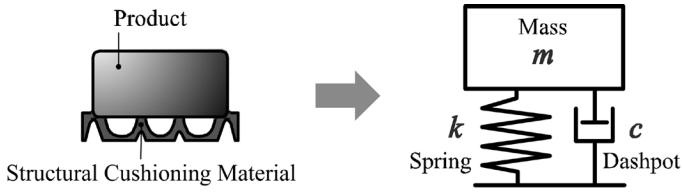

Figure 3. *Viscous damping (VD) model.*

applicable for SCM. The buffer mechanism of SCM is more complex than that of quasi-linear cushioning materials; thus, the factors of viscous damping and linear spring considered in the VD model may not be enough to explain the shock response of the more complex SCM.

Therefore, it is necessary to develop a new model to explain this new phenomenon. In our study, a new physical model that considers both friction and viscous damping was proposed. To validate the model, a half-sine pulse was used as the input acceleration and mathematical simulations were performed. Next, a mathematical equation for the shock response of the new model was deduced by using the simulation code, "Maple", and "MapleSim". Finally, the new model was compared with the VD model using the experimental data.

NEW PHYSICAL MODEL

Based on insights from material mechanics, physics, and the aforementioned analysis, a new model is proposed, as shown in Figure 4(a). It is a combination of mass, two linear springs, damping, and friction. This model is called the frictional-viscous damping model and is abbreviated as "FVD model" in our study.

This new model is based on the following reasoning:

1. Perfect elastic cushioning materials do not exist. Therefore, the effect of attenuation should be considered.

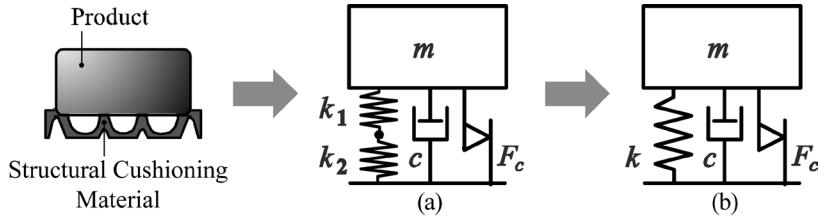

Figure 4. *Frictional-viscous damping (FVD) model. (a) Original FVD model; (b) Simplified FVD model.*

2. Comparison of the peak shock responses of curves C1 with C3 suggests that softer springs should be used in the new model because the shock response of SCM is much smaller than that of EPE.

   Furthermore, two springs in series are considered for the new model because of the stress–strain characteristics of EPE and SCM, as shown in Figure 5(a). Note that the stress–strain curve of EPE is close to a smooth line through the origin; however, the stress–strain curve of SCM increases sharply at 3% strain and then slowly decreases to approximate a horizontal line. Figure 5(a) can be generalized to Figure 5(b). In Figure 5(b), the horizontal axis is the displacement, the vertical axis is the force, and the slopes of the lines are the values of the spring constants. Region A represents the shock energy that EPE can absorb and Region B represents the shock energy that SCM can absorb. To find the spring constant of SCM $k_{(\mathrm{SCM})}$ that equals that of EPE $k_{(\mathrm{EPE})}$, the area of Region B should equal that of Region A. Therefore, the following relationship is obtained:

$$k_{(\mathrm{SCM})} = \frac{k_{(\mathrm{EPE})}}{2} \quad \rightarrow \quad k_c = \frac{k_{(\mathrm{calculated\ value})}}{2} \tag{1}$$

3. The middle region of the SCM shock response curve changes to a trapezoidal shape with no obvious unique peaks probably because of friction. If it is assumed that a pure friction model [Figure 6(a)] describes the cushioning material and an impact pulse is applied for an extremely short duration, then mechanics allows us to obtain the shock response curve for this model [Figure 6(b)]. Note that friction causes a step-wise change in the acceleration.

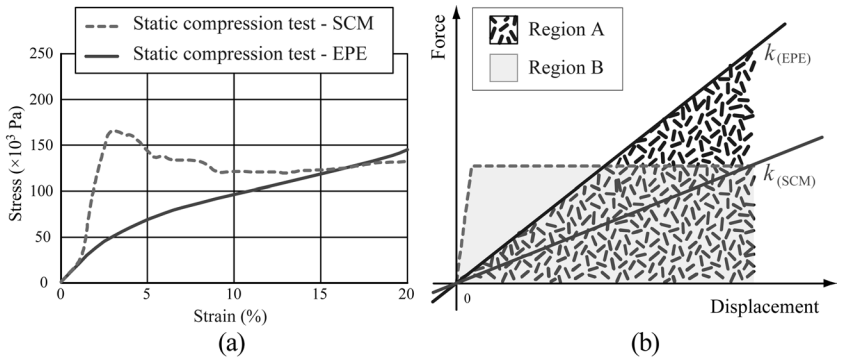

Figure 5. *Stress-strain and displacement-force curves of EPE and SCM. (a) Stress-strain curves; (b) Displacement-force curves.*

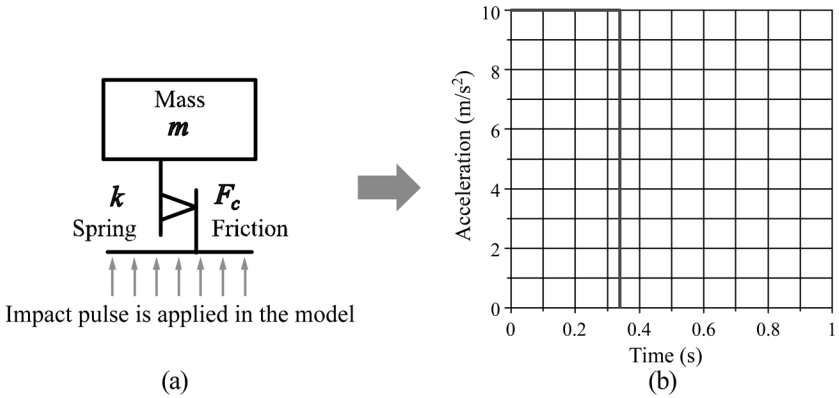

Figure 6. *Effect of friction. (a) Pure friction model; (b) Acceleration—time curve of the pure friction model.*

According to mechanics, two springs in series can be equated to one spring, thus model (a) in Figure 4 can be simplified to model (b) in Figure 4 [3]. The spring constant of two springs in series obeys the following relationship:

$$k = \frac{1}{\frac{1}{k_1} + \frac{1}{k_2}} \tag{2}$$

where k_1 and k_2 are the original spring constants of each spring. If $k_1 = k_2$, then Equation (2) becomes

$$k = \frac{k_1}{2} = \frac{k_2}{2} \tag{3}$$

Therefore, half of the calculated value of spring constant k should be used in FVD model.

SIMULATION OF THE SHOCK RESPONSE OF THE FVD MODEL

MapleSim (Maplesoft Inc., Canada) is a physical modeling tool built on a foundation of symbolic computation technology. It has been widely used in many fields such as automobile manufacturing and aerospace [4]. It can also be used in the packaging field.

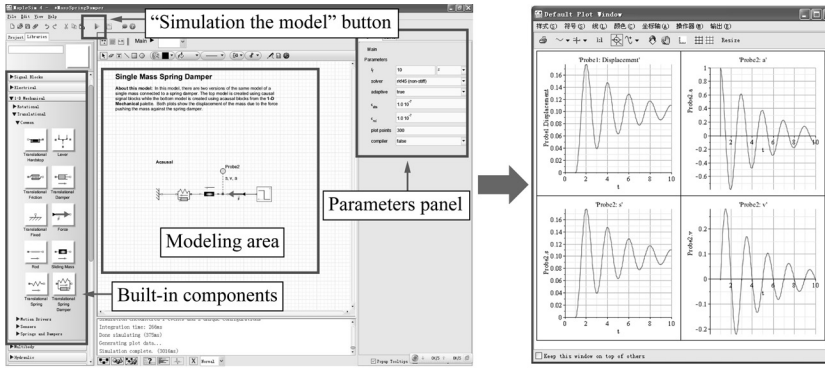

(a) (b)

Figure 7. *MapleSim window and simulation results. (a) MapleSim window and software panels; (b) Simulation results.*

The MapleSim window is shown in Figure 7(a). The simulation procedure is as follows. First, built-in or custom components are used to build a physical model. Second, appropriate parameters are set for each component. Third, a model simulation is performed using the button called "simulation the model" and the simulation results shown in Figure 7(b) are obtained.

Building the Friction Component

Although there are several types of friction, Coulomb friction is used in our study and is defined by

$$F_c = \begin{cases} \mu N \cdot \text{sign}(\dot{x}) & \dot{x} > 0 \\ F_a & \dot{x} = 0 \text{ and } F_a < \mu N' \end{cases} \tag{4}$$

where F_c is the Coulomb friction, μ is the coefficient of friction, N is the normal force exerted between the surfaces, F_a is the force exerted by friction, and $\dot{x}$ is the velocity.

There is a built-in friction component called "translational friction" in MapleSim; however, this friction approximates the sum of Stribeck friction and Coulomb friction [5]. This component does not meet the requirements of our study, thus a custom friction component is defined in Maple on the basis of Equation (4). Its definition is expressed by Equation (5).

$$eq := \left[f(t) = \begin{cases} F_c \cdot \begin{cases} 1 & vrel(t) > 0 \\ -1 & vrel(t) < 0 \end{cases} & |vrel(t)| > vth \\ 0 & |vrel(t)| \le vth \end{cases}, \; srel(t) = sb(t) - sa(t), \right.$$

$$\left. vrel(t) = \frac{d}{dt} srel(t), \; f(t) = fb(t), \; fa(t) + fb(t) = 0 \right] \tag{5}$$

FVD Model

Two FVD models with different input pulses were built on the basis of the model in Figure 4(b), as shown in Figure 8. Figure 8(a) is the model for a half-sine input pulse and Figure 8(b) is the model where the input pulse is the actual waveform. Here component ① is the mass, ② is the damp–spring, ③ is the custom friction, ④ is for converting the data of components ⑤ and ⑥ to acceleration, ⑤ and ⑥ represent the input pulses, and the component labeled "Probe" is to measure the shock response of the model.

For both models, the parameters are set as shown in Figure 9. The spring constant k (c in MapleSim) and the damping coefficient c (d in MapleSim) can be calculated using the experimental data by the equations $k = m\omega_n^2$ and $c = 2\xi\sqrt{km}$, where ξ is the damping ratio. Here $k/2$ is used. The actual waveform data shown in Figure 9-⑥ is applied for component ⑥ in Figure 8. To compare the simulation result with that

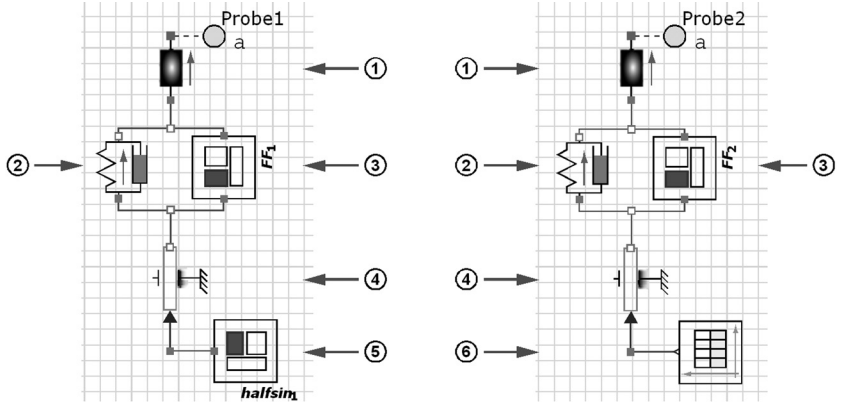

Figure 8. *FVD models in MapleSim. (a) Input pulse is a half-sine waveform; (b) Input pulse is the actual waveform.*

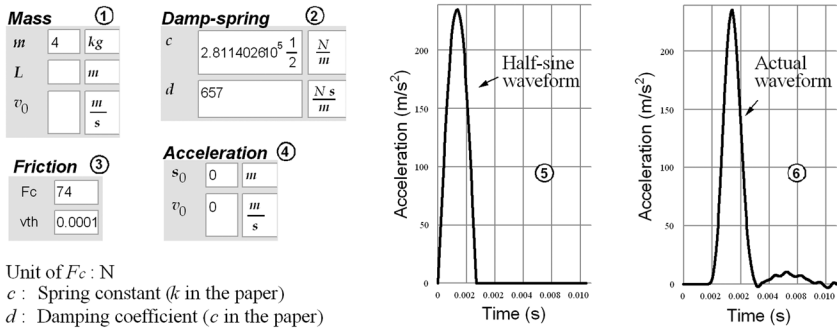

Figure 9. *Parameters of the components of the FVD model with two different input waveforms.*

of the experiment, the parameters of component ⑤ in Figure 8 are set equal to the actual waveform data of the experiment and its diagram is shown in Figure 9-⑤.

Calculating Friction

To simulate the shock response, the friction must be given a specific value. Usually, the positive pressure method approach is used to calculate Coulomb friction; however, this approach cannot be employed in this study because of the structure of SCM. Therefore, based on the principle of conservation of energy, a hysteresis loop [6] is applied to calculate friction.

Hysteresis is a phenomenon that "even if the external force is returned to the initial state, the system can not restore to its original state completely" [6]. Hysteresis can be observed in many materials; for instance, it is found in springs when the applied plastic deformation force is larger than its elastic deformation limit. Furthermore, it is found in structural cushion produced from a corrugated board. If the displacement of a system with hysteresis is plotted against the applied force, the resulting curve is in the form of a loop and is called a hysteresis loop [6].

The shape of a hysteresis loop depends on the physical properties of the material. The shapes of the hysteresis loops for different cushioning materials can be divided into three mass-spring damping models (Figure 10). In Figure 10, the *x*-axis is displacement and the *f*-axis represents force. Model (a) shows the hysteresis loop for the VD model, model (b) shows that for the Coulomb damping model, and model (c) shows that for the Coulomb-viscous damping model. The loss energy

of each model is determined by the area enclosed by its hysteresis loop. Therefore, the loss energy of the models in Figure 10 is as follows:

for (a):

$$E_c = \pi c \omega_n A^2 \tag{6}$$

for (b):

$$E_F = 4F_c A \tag{7}$$

for (c):

$$E_n = \pi c \omega_n A^2 + 4F_c A \tag{8}$$

where ω_n is the natural angular frequency and A is the amplitude of the displacement equation of the system.

If the FVD model is equivalent to the VD model, the equivalent loss energy E_{eq} can be expressed as

$$E_{eq} = \pi c_{eq} \omega_n \tag{9}$$

where c_{eq} is the equivalent damping coefficient under the loss energy.

Let Equation (8) be equal to Equation (9), then F_c can be obtained as shown in following equation:

$$F_c = \frac{\pi}{4}(c_{eq} - c)\omega_n A \tag{10}$$

Here, c_{eq} can be calculated by simulating the VD model in MapleSim

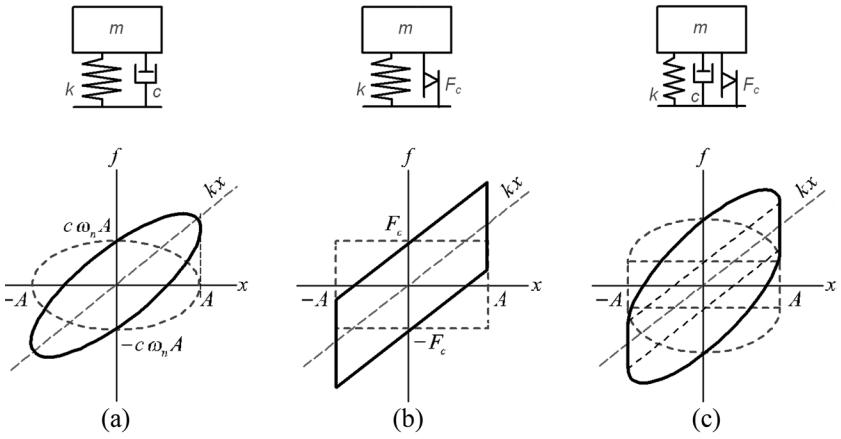

Figure 10. *Hysteresis loop curves of three damping models. (a) VD model; (b) Coulomb damping model; (c) Coulomb-viscous damping model.*

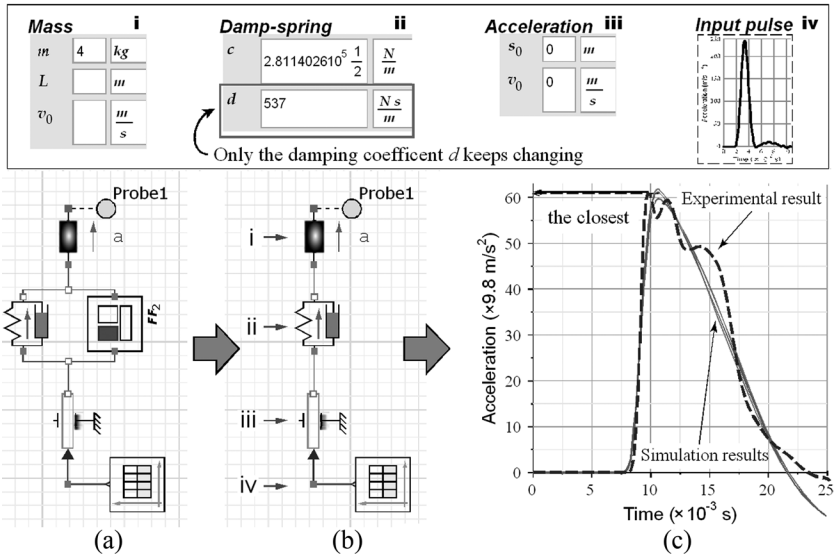

Figure 11. *Calculation of friction. (a) FVD model; (b) Equivalent VD model, top of the figure shows the parameter of each component of this model; (c) Comparison of simulation results and experiment result.*

using experimental data. The calculation produce is described as follows:

Because friction is also a type of attenuation [3], the FVD model [Figure 11(a)] can be equal to a VD model [Figure 11(b)]. Using this equivalent VD model, simulations are performed using MapleSim. Here only c keeps changing, the other parameters m, k are specified with the calculated value and remain unchanged, and the input pulse is

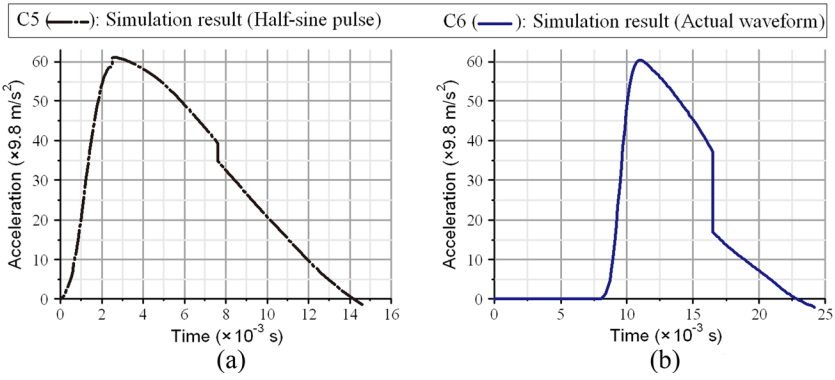

Figure 12. *Simulation results for the FVD models. (a) Input pulse is a half-sine waveform; (b) Input pulse is the actual waveform.*

the same as that in FVD model. Thus, the different simulation curves are obtained [Figure 11(c)] and c is recorded as c_{eq} when the peaks of the simulation curves is closest to the nearest experimental data. An example is as follows:

$$F_c = \frac{\pi}{4}(c_{eq} - c_0)\omega_n A =$$

$$\frac{\pi}{4} \times (537 - 509)\left(\frac{\text{Ns}}{\text{m}}\right) \times 265\ (\text{Hz}) \times (12.6 \times 10^{-3})\ (\text{m}) \doteq 74\ (\text{N})$$

Simulation Results for the FVD Model

The simulation results are shown in Figure 12. Curve C5 is the result for the half-sine wave input, and curve C6 is that for an actual waveform input. The simulation curves are discontinuous and are no longer similar to the half-sine pulse curve: This is considered to be owing to the presence of friction. To accurately express the physical property of friction, the function was introduced. This function changes to a plus or minus $\text{sign}(\dot{x})$ according to the direction of vector $\dot{x}$. Thus, the value of the force will change when the direction of the velocity is altered.

MATHEMATICAL SOLUTION FOR THE SHOCK RESPONSE OF THE FVD MODEL

The FVD model is a nonlinear system because of the factor of coulomb friction, and it is very difficult to precisely solve nonlinear systems. However, there are many methods for approximating the solutions of a nonlinear system [7]. Therefore, the following approach is used for the shock test. First, the equivalent spring constant k_e and the equivalent damping coefficient c_e are calculated using the equivalent linearization method [8]. Second, based on the equation of motion of the FVD model expressed by k_e and c_e, the Laplace transform and the inverse Laplace transform are applied to derive the mathematical solution for the new model.

Equivalent Linearization Method

To minimize the error of the square integral of the equivalent lin-

earization method in one cycle, the evaluation function J is introduced and defined by

$$\begin{aligned} J &= \int_0^{2\pi} [f(x,\dot{x}) - (c_e\dot{x} + k_e x)]^2 \mathrm{d}\theta \\ &= \left[\int_0^{2\pi} (f(x,\dot{x}))^2 \mathrm{d}\theta - 2aAc_e \int_0^{2\pi} f(x,\dot{x}) \cos\theta \mathrm{d}\theta - 2Ak_e \right. \\ &\quad \left. \int_0^{2\pi} f(x,\dot{x}) \sin\theta \mathrm{d}\theta + \pi a^2 A^2 c_e^2 + \pi A^2 k_e^2 \right] \end{aligned} \tag{11}$$

Because J is a function that relates to k_e and c_e,

according to $\dfrac{\partial J}{\partial K_e} = 0$,

$$K_e = \frac{1}{\pi A} \int_0^{2\pi} f(A\sin\theta,\ Aa\cos\theta) \sin\theta \mathrm{d}\theta, \tag{12}$$

and according to $\dfrac{\partial J}{\partial C_e} = 0$,

$$C_e = \frac{1}{\pi Aa} \int_0^{2\pi} f(A\sin\theta,\ Aa\cos\theta) \cos\theta \mathrm{d}\theta, \tag{13}$$

The equation of motion of the FVD model can be expressed as

$$m\ddot{x} + c\dot{x} + kx + F_c\ \mathrm{sign}(\dot{x}) = A\sin at, \tag{14}$$

where x is the displacement, $\dot{x}$ is the velocity and $\ddot{x}$ is the acceleration. Therefore, $f(x,\dot{x})$ is expressed as

$$f(x,\dot{x}) = c\dot{x} + kx + F_c \mathrm{sign}(\dot{x}) = c\dot{x} + kx + F_c \frac{\dot{x}}{|\dot{x}|}. \tag{15}$$

Substituting Equation (15) in Equations (12) and (13), k_e and c_e are obtained as follows:

$$k_e = k, \qquad c_e = c + \frac{4F_c}{\pi Aa}, \tag{16}$$

where $a = \pi/T_0$ and T_0 is the initial impact duration.

Laplace Transformation and Inverse Transformation

The procedure for calculating the mathematical solution is as follows:

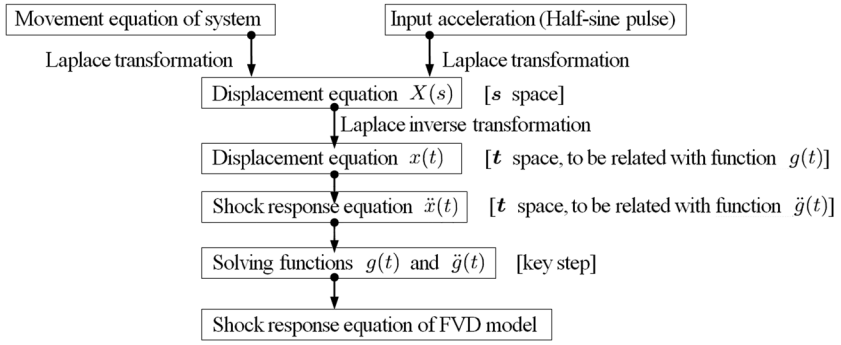

First, the equation of motion of the shock test can be expressed by

$$m\ddot{x} + ce(\dot{x} - \dot{x}_0) + k_e(x - x_0) = 0 \tag{17}$$

Substituting k_e and c_e in Equation (17), the following equation is obtained

$$m\ddot{x} + \left(c + \frac{4F_c}{\pi Aa}\right)(\dot{x} - \dot{x}_0) + k(x - x_0) = 0 \tag{18}$$

After the Laplace transformation is applied, the displacement equation $X(s)$ expressed in space s is

$$X(s) = \frac{(2\omega_n\xi + B)s + \omega_n^2}{s^2 + (2\omega_n\xi + B)s + \omega_n^2} \cdot X_0(s), \tag{19}$$

where $B = 4F_c/(\pi mAa)$ and A_0 is the input acceleration.

In addition, the Laplace transform of the half-sine input acceleration is given by

$$\ddot{x}_0 = A_0\left[\sin\frac{\pi}{T_0} \cdot U(t) - \sin\frac{\pi(t - T_0)}{T_0} \cdot U(t - T_0)\right] \tag{20}$$

where $U(t)$ is a step function and T_0 is the period of the half-sine pulse.

Substituting Equation (20) in Equation (19), the displacement equation can be rewritten as

$$X(s) = \frac{(2\omega_n\xi + B)s + \omega_n^2}{s^2 + (2\omega_n\xi B)s + \omega_n^2} \cdot \frac{A_0 a(1 + e^{-T_0 s})}{s^2(s^2 + a^2)} \tag{21}$$

Next, Laplace transformation with higher-order poles is performed on Equation (21), and function $g(t)$ is obtained as follows:

$$\begin{aligned} g(t) = {} & \frac{1}{a^2}t + \frac{(2\omega_n\xi + B)s + \omega_n^2}{\alpha^2(\alpha - \beta)(\alpha^2 + a^2)}e^{\alpha t} + \frac{(2\omega_n\xi + B)s + \omega_n^2}{\beta^2(\beta - \alpha)(\beta^2 + a^2)}e^{\beta t} \\ & + \frac{\omega_n^2 - ia(2\omega_n\xi + B)}{i2a^3(\alpha + ia)(\beta + ia)}e^{-iat} + \frac{\omega_n^2 - ia(2\omega_n\xi + B)}{-i2a^3(-\alpha + ia)(-\beta + ia)}e^{iat}, \end{aligned} \tag{22}$$

where $a, \beta = -(\omega_n\xi + B/2) \pm i\, Q/2,\ Q = \sqrt{4(\omega_n^2 - \omega_n^2\xi^2 - \omega_n\xi B) - B^2}$, and i is the imaginary unit. Then the second differential of Equation (22) is taken, and function $\ddot{g}(t)$ is obtained as follows:

$$\begin{aligned} \ddot{g}(t) = {} & \frac{(2\omega_n\xi + B)\alpha + \omega_n^2}{(\alpha - \beta)(\alpha^2 + a^2)}e^{\alpha t} + \frac{(2\omega_n\xi + B)\beta + \omega_n^2}{(\beta - \alpha)(\beta^2 + a^2)}e^{\beta t} \\ & + \frac{-\omega_n^2 - ia(2\omega_n\xi + B)}{i2a^3(\alpha + ia)(\beta + ia)}e^{-iat} + \frac{\omega_n^2 + ia(2\omega_n\xi + B)}{i2a(-\alpha + ia)(-\beta + ia)}e^{iat}, \end{aligned} \tag{23}$$

A complex compound number analysis is performed, and the solution of is rewritten as follows:

$$\begin{aligned} \ddot{g}(t) = {} & \frac{-2(\omega_n^4 + a^2E)\sin\dfrac{Q}{2}t + 2a^2\left(\omega_n\xi + \dfrac{B}{2}\right)Q\cos\dfrac{Q}{2}t}{Q\left[\omega_n^4 + \left(4\omega_n^2\xi^2 + \dfrac{5}{2}B^2 + 4\omega_n\xi B - 2\omega_n^2\right)a^2 + a^4\right]} \cdot \exp\left(-\left(\omega_n\xi + \frac{B}{2}\right)t\right) \\ & + \frac{[\omega_n^4 + a^2(2\omega_n\xi + B)^2 - a^2\omega_n^2]\sin at - [a^3(2\omega_n\xi + B)]\cos at}{a[\omega_n^4 + a^2(2\omega_n\xi + B)^2 - 2a^2\omega_n^2 + a^4]} \end{aligned} \tag{24}$$

where $E = 2(\omega_n^2\xi^2 + B^2/4 + \omega_n\xi B) - \omega_n^2$.

Finally, the displacement equation of the shock test in space t can be

expressed as Equation (25) after applying the second transition theorem and performing a Laplace inverse transformation with higher-order poles.

$$x(t) = A_0 a[g(t)\cdot U(t) + g(t-T_0)\cdot U(t-T_0)] = \begin{cases} A_0 a\cdot g(t) & 0<t<D \\ A_0 a\cdot[g(t)+g(t-D) & t>D \end{cases}, \quad (25)$$

where D is the impact duration.

The differential of Equation (25) is performed and the mathematical shock response $A_{cs}(t)$ is obtained as follows:

$$A_{cs}(t) = \ddot{x}(t) = \begin{cases} A_0 a\cdot \ddot{g}(t) & 0<t<D \\ A_0 a\cdot[\ddot{g}(t)+\ddot{g}(t-D) & t>D \end{cases}, \quad (26)$$

where $\ddot{g}(t)$ is expressed by Equation (24).

Plotting the Mathematical Shock Response Curves

According to Equation (26), the key issue is calculating function $\ddot{g}(t)$. For function $\ddot{g}(t)$, ω_n is an important parameters. Here ω_n can be calculated by $\omega_n = \pi/D$, where D is impact duration obtained from the experimental data. Equation (26) is defined in Maple and the correlative coefficients are calculated using the experimental data. Thus, the mathematical shock response curve of the FVD model can be plotted, as shown in Figure 13.

```
eq1:=eval(eq1, {A0 = 257.5, a = 1481, ω = 189, ξ = 0.299, B = 83, Q = 326, E = -17544, D = 0.00212}):
plot (eq1, t = 0 . . 0.02, -5 . . 65)
```

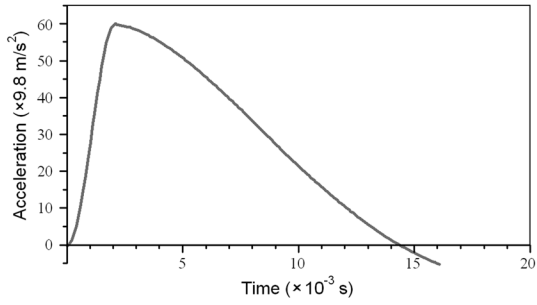

Figure 13. *Mathematical shock response curve of FVD model. The top of the figure shows a screenshot of each parameter in Maple.*

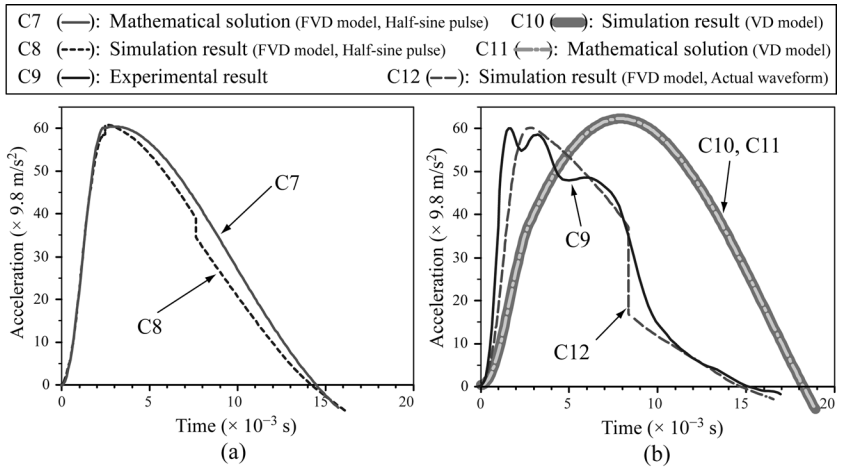

Figure 14. *Comparison of shock response curves.*

RESULTS AND DISCUSSION

Figure 14 summarizes the aforementioned shock response curves. Each curve is described as follows:

- Curve C7 is the mathematical shock response curve calculated from Equation (26) on the basis of the FVD model; it is the same curve as that shown in Figure 13.
- Curve C8 is the simulation shock response curve based on the FVD model using the half-sine wave as the input pulse; it is the same curve as that shown in Figure 12(a).
- Curve C9 is the shock response curve for the experimental shock test under the following conditions: the sleeve in Figure 2(a) is used as the test material, $m = 4$ kg, drop height $h = 0.6$ m (the initial impact velocity v_0 can be calculated as 3.43 m/s by the equation $v_0 = \sqrt{2gh}$, where g is the acceleration of gravity) and the input pulse in Figure 9-⑥ serves as the input acceleration.
- Curve C10 is the simulation shock response curve based on the VD model.
- Curve C11 is the mathematical shock response curve based on the VD model; it is the same curve as C4 shown in Figure 2(b).
- Curve C12 is the simulation shock response curve based on the FVD model with the actual waveform as the input pulse; it is the same curve as that in Figure 12(b).

To facilitate ocular comparison, the zero-acceleration data from curves C3 in Figure 2(b) and C6 in Figure 12(b) are eliminated when plotting curves C9 and C12. Furthermore, $k/2$ is used for the following five curves: C7, C8 , C10, C11 and C12.

Figure 14 illustrates the following points:

- As previously mentioned, the VD model cannot suitably determine the shock response of SCM. This conclusion is validated by comparing the experimental shock response curve (C9) with the VD model simulation (C10) and mathematical (C11) shock response curves.
- The FVD simulation curves (C8 and C12) are discontinuous. This discontinuity is probably caused by the presence of friction.
- The FVD mathematical (C7) and simulation (C8) shock response curves for the half-sine wave input acceleration are similar but not identical. This discrepancy is probably caused by the equivalent linearization method in the mathematical analysis, which leads to a precision error.
- The input accelerations are different between Figure 14(a) and Figure 14(b); consequently, the FVD shock response curves C7 and C8 need not exactly match the experimental shock response curve C9. Nevertheless, a comparison of Figure 14(a) with Figure 14(b) shows that both curves C7 and C8 differ from the VD shock response curves C10 and C11, and they are similar to the experimental shock response curve C9.
- Curve C12 is closer to the shape of the experimental curve C9 compared with curves C7 and C8 because the actual input waveform for C12 is identical to that used in the experiment, whereas it is a half-sine wave for curves C7 and C8.

CONCLUSION

The VD model is not applicable for SCM has been demonstrated in our study. Therefore, a new physical model considering a factor of friction was proposed. Using this new model, a shock response equation of shock test was deduced.

To specify the value of the friction, a new friction equation was derived on the basis of the principle of the conservation of energy and a hysteresis loop. Meanwhile, a new method to calculate the damping ratio was proposed by conducting simulations in “MapleSim”.

The reliability of the proposed FVD model was checked by comparing the results of simulations and the experiment. The result shows that the shock response determined by the FVD model approximates the data more accurately than the conventional VD model for SCM.

REFERENCES

1. Chen ZHONG and Katsuhiko SAITO: "Modified Simulated Drop Test for Transmitted Shock Characteristics of Structural Corrugated Fiberboard", *Journal of Applied Packaging Research,* Vol. 4, No. 4, pp.189–201 (October, 2010).
2. Chen ZHONG and Katsuhiko SAITO: "Equivalent Drop Test Modification for Determination of Cushioning Performance", *Journal of Packaging Science & Technology,* Japan, Vol. 19, No. 2, pp. 123–135 (2010).
3. Singiresu S. Rao. *Mechanical Vibrations (5th Edition),* Pearson Education (September, 2010).
4. MapleSim 4.5, <http://www.maplesoft.com/products/maplesim/index.aspx> (accessed August 2011).
5. *MapleSim User's Guide,* MapleSim Ver. 4.5, Maplesoft Co. Ltd..
6. Keith R. Symon. *Mechanics (3rd Edition),* Addison Wesley (January, 1971).
7. Cyril M. Harris, Allan G. Piersol. *Harris' Shock and Vibration Handbook (Fifth Edition),* McGraw-Hill (2002).
8. S. Bran, D. Ewins, S. S Rao. *Encyclopedia of Vibration,* Academic Press (2002).

Evaluation Study of Vanillin, Curcumin and Turmeric with Potential Use in Antimicrobial Packaging Applications

YUJIE CHENG[1,*], CHANGFENG GE[2], JEFFREY LODGE[3] and K.S.V SANTHANAM[1]

[1]*Department of Material Science, Rochester Institute of Technology*
[2]*Department of Packaging Science, Rochester Institute of Technology*
[3]*Department of Biological Science, Rochester Institute of Technology*

ABSTRACT: This study investigated the antimicrobial effects of vanillin solutions, turmeric solutions and curcumin solutions for potential packaging coating applications. The coating solutions involving these three antimicrobial agents are: vanillin/ reagent alcohol (10, 5, 2.5 and 1.25% (w/w)), turmeric/reagent alcohol (10, 5, 2.5 and 1.25% (w/w)) and curcumin/reagent alcohol (10, 5, 2.5 and 1.25 (w/w)). The antimicrobial activity effects of the aforementioned coating solutions were investigated for five types of common pathogens and food spoilage bacteria: *Staphylococcus aureus* and *Listeria monocytogenes* representing gram-positive bacteria; *Shigella sonnei*, *Salmonella choleraesuis* as well as *E. Coli* (O157:H7) representing gram-negative bacteria. Significant antimicrobial effects for gram-positive bacteria were observed for curcumin/reagent alcohol solutions and turmeric/reagent alcohol solutions. It is also noticed that gram-negative bacteria were more sensitive over vanillin/ reagent alcohol solutions. However, at higher concentration (10%(w/w) and 5%(w/w)), turmeric and curcumin were not completely soluble in reagent alcohol. The insoluble particles prevent the migration of the turmeric and curcumin into solutions, which result in a minimization of the zone of inhibition. Future research is suggested to focus on an alternate solvent, which has better solubility for curcumin and turmeric, instead of reagent alcohol.

1. INTRODUCTION

ANTIMICROBIAL AGENTS are chemicals that are used against bacteria. There are many natural agents available in the market. Antimicrobial packaging is gaining interest from researchers and industry due to its potential to provide quality and safety benefits.

*Author to whom correspondence should be addressed.

1557-7244/11/04 215-12

Antimicrobial packaging is a form of active packaging, which acts to reduce, inhibit or retard the growth of microorganisms that may be present in the packed food or packaging material itself [1]. The next generation of food packaging may include materials with antimicrobial properties. These packaging technologies could play a role in extending shelf-life of foods and reduce the risk from pathogens [10]. The typical materials applied in antimicrobial food packaging including paperboard as well as LDPE, HDPE, Chitosan, PE, silicon coating and so on [2]. In addition, since paperboard has so many useful properties and can be used as antimicrobial material in food packaging, it is possible that coating antimicrobial agents on paperboard and used in packaging can extend the shelf-life of the product.

Natural plants, which have antimicrobial agents are widely used in ethno-medicine around the world can dating back to thousand years ago. In the first century A.D., Dioscorides wrote De Materia Medica, which offers descriptions of approximately 30 healing plants. However, since the development of antibiotics in 1950s, the use of antimicrobial agents derived from plants became seldomness [4]. Currently, the natural plants with antimicrobial activity come back to our life: essential oil such as Cinnamomum zeylanicum, Thymus vulgaris and Origanum vulgaris were studied as antimicrobial solutions in paper packaging [9]. There are many advantages by using natural plants as antimicrobial agents: firstly, it is cheap especially for use in underdeveloped nations with little access to expensive western medicines; secondly, natural agents without any chemical synthetic products should be more safe and have less side effects. Thus, it is possible and effective to coating these natural plants powder on packaging materials in order to extend the self-life of products.

Vanillin has been selected as an antimicrobial agent for coating paperboard intended for packaging bakery products. Suwarat Rakchoy, *et al.* [3] evaluated the inhibitory effects of vanillin coated solutions and investigated minimum inhibitory concentration of the solution against selected bacteria including *Escherichia coli, Staphylococcus aureus* and Bacillus cereus. Furthermore they assessed the self-life of vanillin coating paperboard with bakery product, and the results showed that the shelf-life was extended compared with the uncoated paperboard. The chemical structure of vanillin is shown in Figure 1.

Turmeric, a bright yellow-orange substance, obtained from the root of the plant Curcuma longa, has long been used as a traditional spice in both China and Indian. Turmeric is mostly used in flavored milk drinks,

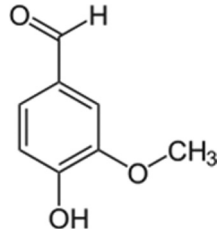

Figure 1.

cultured milk and desserts to obtain lemon and banana colors in dairy. In the previous research, turmeric has been shown to have anti-HIV activity [4], anti-cancer [5] activity as well as antimicrobial activity [6]. Turmeric contains up to 5% essential oils and up to 3% curcumin, a polyphenol. The main components of turmeric are: curcumin (60%), desmethoxycurcumin, monodemethoxycurcumin, bisdemethoxycurcumin, dihydrocurcumin and cyclocurcumin [13]. The Structure of the main curcuminoids of turmeric is shown in Figure 2.

Curcumin is the most biologically active constitute of turmeric. The chemical structure of curcumin is shown in Figure 3. The characteristic yellow color of turmeric is due to curcumin [7]. Antimicrobial activity of curcumin against S. aureus and S.epidermidis as well as minimum inhibitory concentration (MIC) has been reported by Saeed Tajbakhsh *et al.* [8]. It was reported that curcumin inhibits the growth of varieties

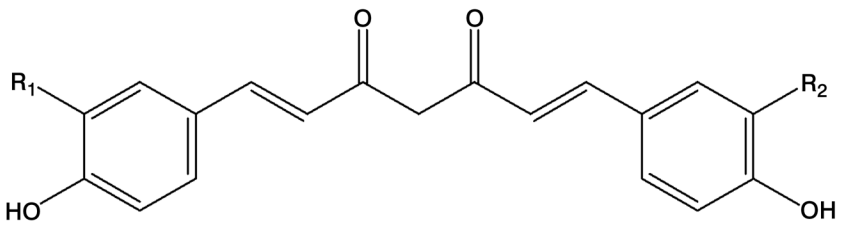

	R_1	R_2
Curcumnia	OCH_3	OCH_3
Desmetoxicurcumnia	H	OCH_3
Bisdesmetoxicurcumnia	H	H

Figure 2. *[13].*

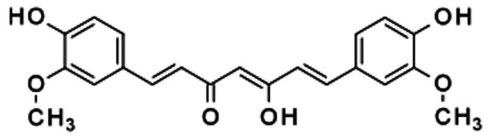

Figure 3. *Chemical structure of curcumin.*

of microbes such as viruses, bacteria and some pathogenic fungi [12]. In some other studies such as indium curcumin and microcapsule curcumin, the antimicrobial effects had been reported for particular bacterial [8,11]. For this study, different concentration of vanillin, turmeric and curcumin reagent alcohol solutions were prepared. The aim of the study was to evaluating the inhibitory effects of three different kinds of solutions against selected bacteria including: *E. Coli* (O157:H7), *Staphylococcus aureus*, *Shigella sonnei*, *Salmonella choleraesuis*, and *Listeria monocytogenes.*

2. MATERIALS AND METHODS

2.1 Bacterial Stains

Five types of common pathogenic and food spoilage bacteria were selected. They are (a) gram-positive bacteria: *Staphylococcus aureus* and *Listeria monocytogenes*; (b) gram-negative bacteria: *Shigella sonnei*, *Salmonella choleraesuis*, *E. Coli* (O157:H7). All bacterial strains were provided by the Department of Biological Sciences, Rochester institute of technology, NY, U.S.

2.2 Reagents and Solvents

Turmeric powders were obtained from supermarket. Vanillin and crucumin was obtained from Sigma-Aldrich Co. LLC. U.S..

The solvent used is Reagent Alcohol (water 0.5% max; residue after evaporation: 0.001% max; ethanol + methanol 94.0–96.0%; isopropyl alcohol 4.0–6.0%; color APHA) was also obtained from Sigma-Aldrich Co. LLC. U.S..

2.3 Preparation of Solutions

Three types of solution were prepared including turmeric/reagent alcohol, curcumin/reagent alcohol and vanillin/reagent alcohol. All these

three solutions were prepared by diluting the powder directly with reagent alcohol, in a series of half-fold dilutions, 10%, 5%, 2.5% and 1.25% (w/w).

2.4 Antimicrobial Testing

The antimicrobial activities of vanillin, turmeric and curcumin solutions were analyzed on Mueller-Hinton II agar (VWR) by diffusion method. Each kind of bacteria was placed onto Mueller-Hinton agar plates by cotton swab. The bacteria of interest were swabbed uniformly across the plate. Using blank antibiotic assay discs of 6mm in diameter, impregnated with 40 µl of vanillin, turmeric and curcumin solutions were placed on the surface of the agar respectively. The solutions diffused out from the antibiotic assay disc into the agar. Then, the plates containing the testing samples were incubated in an environment for 24 h at 35.5°C. Control sample were performed triplicate on each bacterial with 40 µl reagent alcohol. Vanillin, turmeric and curcumin solutions were performed triplicate for different concentrations. In order to obtain comparable results, all prepared solutions were applied under the same conditions and the same incubation environment. The antimicrobial activities of all solutions were detected as clear zones around the antibiotic assay discs, and the diameters of the clear zones are measured in millimeters (mm) by a ruler. If the solution is effective against bacteria at a certain concentration, no colonies will grow wherever the concentration in the agar is greater than or equal to that effective concentration. This region is called the "zone of inhibition." Thus, the size of the zone of inhibition is a measure of the compound's effectiveness. The larger the clear zone around the antibiotic assay disc, the more effective the solution is. The minimum inhibitory concentration (MIC) was defined as the lowest concentration of solutions that completely inhibit the growth of each bacterial and fungal strain being tested [11].

3. RESULTS AND DISCUSSION

3.1 Antimicrobial Effects of Vanillin, Turmeric and Curcumin in Reagent Alcohol Solution

The average diameter and standard deviation of inhibition clear zone of control sample, Vanillin/reagent alcohol solution, Turmeric/reagent alcohol solution and Curcumin/reagent alcohol solution are illustrated

in Table 1. A comparison of antimicrobial activity of different solution over particular microorganisms is shown in Figure 4(a)-(e). Furthermore, clear zone diameters for types of solution over five microorganisms also illustrated in Figure 5(a)-(e).

If there was no distinct inhibition clear zone observed in the test, the diameter is marked as "na". Standard deviation is "na" illustrated that there were no distinct inhibition clear zone observed in three replicates.

According to the results in Table 1, vanillin/reagent alcohol solution is more effective over *E. Coli* with a minimum inhibitory concentration (MIC) at 2.5% (w/w). The results agree with previous studies on the effect of vanillin/alcohol solution in inhibiting *E. coli* [3]. In addition, vanillin/reagent alcohol solution has significant effectiveness on *Shigella sonnei* and *Listeria monocytogenes* with the MIC at 2.5% (w/w). Whereas the same solution has slight less antimicrobial activity on *Staphylococcus aureus* and *Salmonella choleraesuis*. The results contradict previous study on the effect of vanillin/alcohol solution in inhibiting *E. Coli* by Jinkarn et al. [3] who reported that vanillin/alcohol was more effective over *Staphylococcus aureus*.

Turmeric/reagent alcohol solution has a weak antimicrobial activity on *Staphylococcus aureus* and *Listeria monocytogenes* with the MIC at 10% (w/w). This finding is in the agreement with Chaudhary *et al.* [13] who reported the turmeric alcohol extract has anti-bacterial activity against Gram-positive bacteria. However, turmeric/reagent alcohol solution has no significant antimicrobial effect on *E. Coli, Shigella sonnei* and *Salmonella choleraesuis*. The antimicrobial activity of turmeric/reagent alcohol has some antimicrobial effective on Gram-positive bacteria, but appears no significant antimicrobial effect on Gram-negative bacteria.

As the most biologically active constitute of turmeric, curcumin has significant antimicrobial activity over *Staphylococcus aureus* and *Listeria monocytogenes*. According to the results, the MIC of curcumin/reagent alcohol solution was valued at 2.5% (w/w) for *Staphylococcus aureus*, but was only 1.25% (w/w) for *Listeria monocytogenes*. However, based on the results, curcumin has no significant effect on Gram-negative bacteria: *E. Coli, Shigella sonnei* and *Salmonella choleraesuis*. In summary, the results indicated that the selected Gram-positive bacteria had higher sensitivity than the selected Gram-negative bacteria. The results agree with previous studies by Bhawana *et al.* [14] who also reported that such antimicrobial effect with selectivity could be due to differences in their cell membrane constituents and structure. [14]

Table 1.

Bacterial	Control Sample		Concentration (%w/w)	Vanillin		Turmeric		Curcumin	
	Average (mm)	Standard Deviation		Average (mm)	Standard Deviation	Average (mm)	Standard Deviation	Average (mm)	Standard Deviation
E. Coli (O157:H7)	12.33	2.89	10	22.00	0	6.50	0.71	na	na
			5	15.00	1.00	na	na	8.67	1.53
			2.5	12.33	0.58	7.67	2.08	10.33	2.08
			1.25	11.67	1.53	11.33	3.79	13.00	2.00
Staphylococcus aureus	9.00	1.00	10	12.33	2.89	14.33	1.53	14.33	1.53
			5	10.00	0	8.33	1.53	17.33	1.53
			2.5	9.67	0.58	9.00	0	25.00	1.73
			1.25	10.00	0	8.67	1.53	9.67	1.15
Shigella sonnei	10.33	0.58	10	18.33	3.79	11.33	3.79	8.33	2.89
			5	16.00	2.00	9.33	5.77	14.67	4.16
			2.5	12.67	1.15	8.00	1.73	17.67	3.51
			1.25	10.67	0.58	9.33	2.31	16.67	3.79
Salmonella choleraesuis	17.67	3.79	10	21.67	1.53	7.33	2.08	12.00	1.00
			5	18.33	1.5	11.33	4.93	10.67	1.15
			2.5	15.33	0.58	11.00	2.65	12.00	1.73
			1.25	14.00	0	10.00	0	12.00	3.46
Listeria monocytogenes	10.00	1.00	10	17.00	1.00	15.67	0.58	11.00	4.00
			5	13.00	0	7.67	0.58	22.67	1.53
			2.5	11.67	1.53	10.33	0.58	23.00	1.00
			1.25	12.00	1.00	11.67	2.08	23.33	1.15

In general, increasing its concentration should intensify the antimicrobial activity of certain powder/reagent alcohol solution. From the results, vanillin/reagent alcohol solution had increasing antimicrobial effect over all five bacterial strains when the concentration increased. The MIC of vanillin/reagent alcohol solution is 2.5% (w/w) over all tested bacterial excepted 5% (w/w) over *Salmonella choleraesuis*. However, the data from turmeric and curcumin demonstrated that a decreasing concentration of solution results in an increased antimicrobial activity. This could be caused by an incompletely soluble of turmeric or curcumin in reagent alcohol. The insoluble particle in turmeric or curcumin reagent alcohol solution might possibly prevent the migration of solution that contained antimicrobial agents. Therefore, when the solution was diluted in lower concentration, there were less insoluble particles and increasing the migration of solution.

3.2 The Influence of Concentration on Antimicrobial Activity Over Each Bacterial

When compared within certain bacterial strain, the three different kinds of solution shown different antimicrobial effect. The influence of Concentration on antimicrobial activity over each bacterial had been presented Figure 4.

Of the selected Gram-negative bacteria in the study [Figure 4(a), (c), (d)], the most effective one is vanillin/reagent alcohol solution at 10% (w/w). Comparing with a clear zone diameter of 12.33 mm for *E. Coli* in control sample, vanillin/reagent alcohol solution had significantly more antimicrobial activity, with a diameter of 22 mm. *Shigella sonnei* and *Salmonella choleraesuis* were also relative more sensitive on vanillin/reagent alcohol solution at 10% (w/w) compared with turmeric and curcumin solution. However, turmeric/reagent alcohol solution and curcumin/reagent alcohol solution had less impact on Gram-negative bacteria in antimicrobial effect. Surprisingly, the inhibition clear zone diameter of turmeric/reagent alcohol solution and curcuim/reagent alcohol solution were smaller than the control sample's. Two factors could contribute this unusual result: interference of solution migration by the insoluble particles in the solution and the large Standard Deviation in the test.

Results from selected Gram-positive bacteria [Figure 4(b), (f)] showed that turmeric/reagent alcohol solution and curcumin/reagent alcohol solution were more effective on *Staphylococcus aureus* and

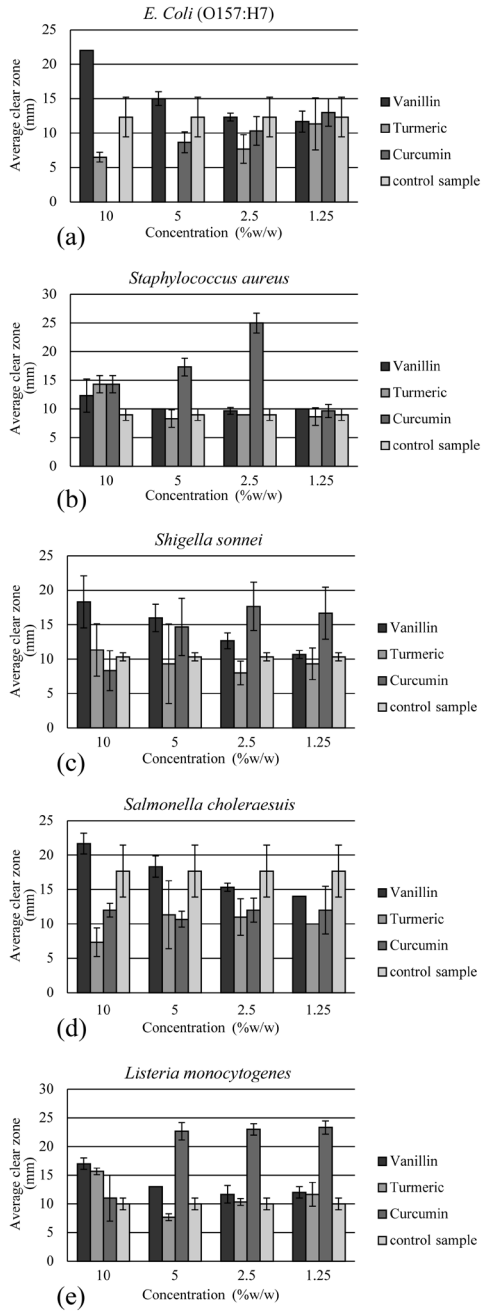

Figure 4. *Antimicrobial activities and MICs of control sample and vanillin, Turmeric, Curcumin in reagent alcohol solutions. (a) E. Coli (O157:H7), (b) Staphylococcus aureus, (d) Salmonella choleraesuis, (e) Listeria monocytogenes.*

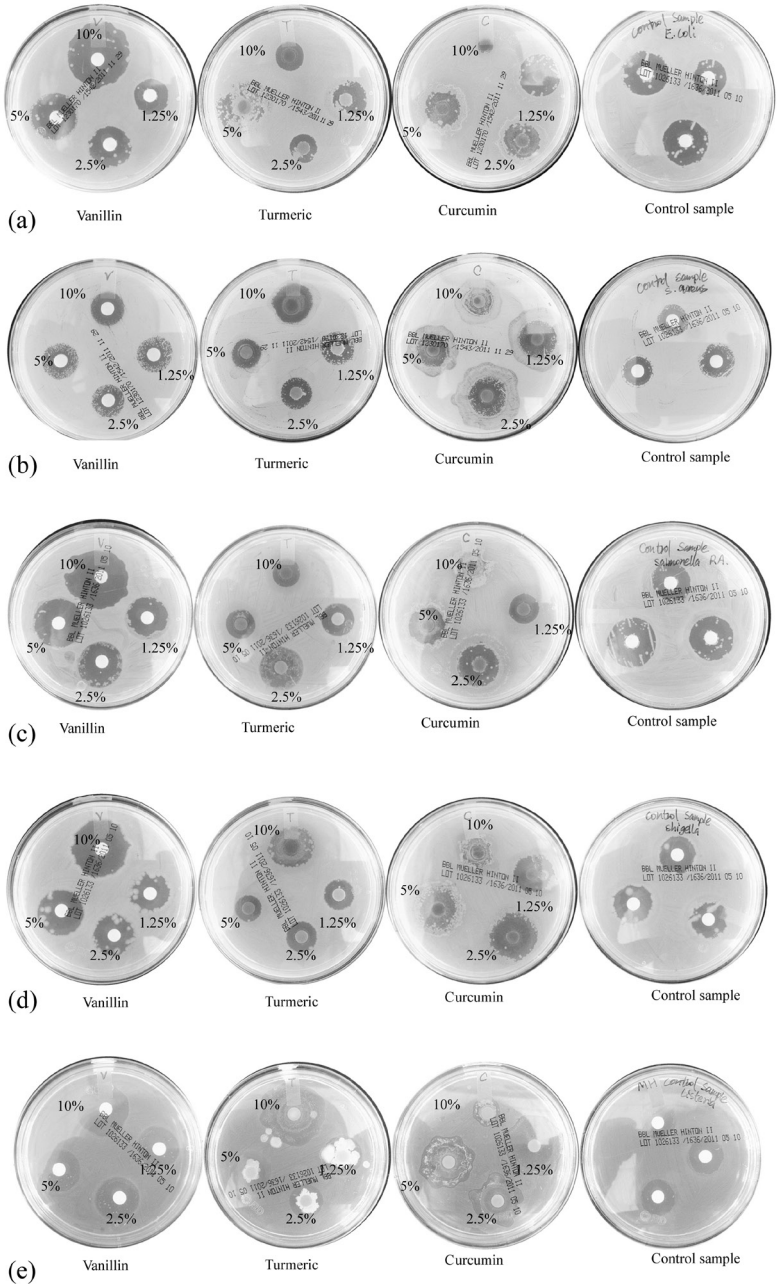

Figure 5. *The illustration above shows zones of inhibition around antibiotic assay discs saturated with 40 µl of vanillin, turmeric and curcumin solutions respectively. (a) E. Coli (O157:H7), (b) Staphylococcus aureus, (c) Shigella sonnei, (d) Salmonella choleraesuis, (e) Listeria monocytogenes.*

Listeria monocytogenes. In Figure 4(b), *Staphylococcus aureus* was significantly inhibited by curcumin/reagent alcohol solution at 2.5% (w/w)that leads to conclude that curcumin/reagent alcohol solution at 2.5% (w/w) was the most effective antimicrobial agent over *Staphylococcus aureus* when compared with vanillin and turmeric. Furthermore, *Listeria monocytogenes* [Figure 4(e)] also revealed higher sensitive on curcumin/reagent alcohol solution, but in a much lower concentration at 1.25% (w/w) as compared with *Staphylococcus aureus*. Turmeric, which also had slightly antimicrobial effect over Gram-positive bacteria, did not shown strong antimicrobial activity as curcumin.

In conclusion, antimicrobial inhibitory of vanillin/reagent alcohol solution have more antimicrobial effect on *E. Coli*, *Shigella sonnei* and *Salmonella choleraesuis* than *Staphylococcus aureus* and *Listeria monocytogenes* in this study. Turmeric/reagent alcohol solution and curcumin/reagent alcohol solution, however, were more effective over *Staphylococcus aureus* and *Listeria monocytogenes*.

4. CONCLUSIONS

Vanillin, turmeric and curcumin are promising natural antimicrobial agent. This study concluded that vanillin/reagent alcohol solutions demonstrated strong antimicrobial effect on three types of common food pathogenic and spoilage Gram-negative bacteria: *E. Coli*, *Shigella sonnei* and *Salmonella choleraesuis*. On the other hand, Gram-positive bacteria: *Staphylococcus aureus* and *Listeria monocytogenes* are more sensitive to curcumin/reagent alcohol and turmeric/reagent alcohol solutions. However, the antimicrobial effect involving reagent alcohol solutions for specific types of bacteria depends on the concentrations of each powder solutions, the insoluble particles in the mixture and the type of bacteria used.

Future work is suggested to focus on minimizing the insoluble particles in the curcumin and turmeric solutions. It is also interesting to study if dimethyl sulfoxide DMSO is applied a solvent to dilute turmeric and curcumin agents, that could lead to an application of antimicrobial paperboard coating in food packaging.

5. REFERENCES

1. Paola Appendini, Joseph H. Hotchkiss, “Review of antimicrobial food packaging,” *Innovative Food Science & Emerging Technologies,* 3 (2002) 113–126.
2. Jung H. Han, “Antimicrobial Food Packaging,” *Food Technology,* March 2000, Vol. 54, No. 3.

3. Suwarat Rakchoy, Panuwat Suppakul and Tunyarut Jinkarn, "Antimicrobial effects of vanillin coated solution for coating paperboard intended for packaging bakery products," *Asian Journal of Food and Agro-Industry* 2009, 2(04), 138–147.
4. Marjorie Murphy Cowan, "Plant Products as Antimicrobial Agent, clinical microbiology review," Oct. 1999, p. 564–582.
5. Goyal, Rajat. The Study of Turmeric as an Effective Antiseptic Agent against Escherichia coli Strain K-12 Bacteria [Internet]. Version 6. Knol. 2010 Feb 18.
6. Seher Gur, Dilek Turgut-Balik and Nazmi Gur, "Antimicrobial activities and some fatty acids of Turmeric, Ginger Root and Linseed Used in the Treatment of infectious diseases," *World Journal of Agricultural Sciences,* 2(4):493–442, 2006.
7. Archana Pandey, Ravindra Kumar Gupta and Roli Srivastava. curcumin-the yellow magic. Department of chemistry, C.M.P. degree college, University of Allahabad, Allahabad 211002, U.P., India.
8. Saeed Tajbakhsh1, Khosro Mohammadi, Iman Deilami, Keivan Zandi, Moradali Fouladvand, Elissa Ramedani and Golandam Asayesh. "Antibacterial activity of indium curcumin and indium diacetylcurcumin," *African Journal of Biotechnology,* Vol. 7 (21), pp. 3832–3835, 5 November, 2008.
9. A. Rodríguez, R. Batlle, C. Nerín , "The use of natural essential oils as antimicrobial solutions in paper packaging. Part II," *Progress in Organic Coatings,* 60 (2007) 33–38.
10. Paola Appendini, Joseph H. Hotchkiss, "Review of antimicrobial food packaging," *Innovative Food Science & Emerging Technologies,* 3 (2002) 113–126.
11. Yu Wang, Zhaoxin Lu, Hao Wu, Fengxia Lv. "Study on the antibiotic activity of microcapsule curcumin against foodborne pathogens." *International Journal of Food Microbiology,* 136 (2009) 71–74. University of Allahabad, Allahabad 211002, U.P., India.
12. Chai, H., S. Yan, P. Lin, A. B. Lumsden, Q. Yao and C. Chen, 2005. "Curcumin blocks HIV protease inhibitor ritonavir-induced vascular dysfunction in porcine coronary arteries." *J. Am. Coll. Surg.,* 200:820–830.
13. Priyanka Chaudhary, Pramod Kumar Sharma, Vipin Kumar Garg, Jonish Varshney. "A review on pharmacological activities of turmeric." *Pharmacologyonline,* 3: 193–199 (2010).
14. Bhawana, Rupesh Kumar Basniwal, Harpreet Singh Buttar, V. K. Jain, and Nidhi Jain. "Curcumin Nanoparticles: Preparation, Characterization, and Antimicrobial Study." dx.doi.org/10.1021/jf104402t | *J. Agric. Food Chem.,* 2011, 59, 2056–20.

The Evaluation of Reusability of Diamond-like Carbon (DLC) Coated PET Bottles with Respect to Gas Barrier and Anti-contamination Properties

AKIRA SHIRAKURA[1,2,*], CHIEKO KUROYANAGI[1,2], YUKIHIRO YOSHIMOTO[2], SO NAGASHIMA[2] and TETSUYA SUZUKI[2]

[1]*Kanagawa Academy of Science and Technology, 3-2-1 Sakado, Takatsu-ku, Kawasaki 213-0012, Japan*

[2]*Center for Environment, Resources and Energy Science, Graduate School of Science and Technology, Keio University, 3-14-1 Hiyoshi, Kohoku-ku, Yokohama 223-8522, Japan*

ABSTRACT: The performance of diamond-like carbon (DLC) coating as a functional barrier for PET bottles in reuse cycle was evaluated.

We have recently developed a technique for coating the inner surface of PET bottles with DLC as a gas barrier to protect the contents and these bottles have been commercialized for soft drinks in Japan. In addition, in terms of the resource protection, reusing of PET bottles is expected as beneficial way with recycling. In this study, the usability of DLC-coated PET bottles in reuse process was investigated.

For assessing the effect of washing, we repeatedly washed bottles with alkaline solution, and then the gas barrier property was evaluated. After 15 times of repeated washing, DLC-coated PET bottles kept its oxygen transmission rate to about one third that of virgin PET bottles. We also evaluated the protection performance of DLC to chemical pollutants. In this study, we prepared polluted virgin and DLC-coated PET bottles with toluene and 1,1,1-tricrolomethane, then measured the migration of contaminants into the food simulants, 4% aqueous acetic acid solution and 50% aqueous ethanol solution, with gas chromatography. The result shows that the contaminants migration to the both food simulants from polluted DLC-coated PET bottles was drastically inhibited and its amount was under one-tenth comparing with virgin PET bottles.

1. INTRODUCTION

OVER the past quarter-century, the plastic food/beverage container production has increased markedly in many countries. Among

*Author to whom correspondence should be addressed. Email: shirakura@kuramae.ne.jp

1557-7244/11/04 227-10

them, polyethylene terephtalate (PET) bottles have been successfully replacing conventional reusable glass bottles. Since PET bottles are mostly used as one-way bottles, their disposal has generated serious environmental issues in major consuming nations including Japan. To address these problems, reuse of post-consumer PET bottles is considered as a beneficial way of reducing the waste and resource consumption together with the recycling, and it is actually introduced in some of European countries. In this paper, "reuse" refers to conventional reuse where the bottles are refilled including collection and washing processes. The reason not to use as rusable bottles worldwide including Japan is absorption behavior of the surface of PET resin unlike glass bottles. Since molecular network of PET has micro space where chemicals can penetrate into inside, PET bottles tend to absorb smelly and dirty matters, and it is hard to remove them by washing with hygienic assurance.

Meantime, Diamond-like carbon (DLC) has attracted much attention and been actively studied owing to its unique characteristics such as high hardness, chemical inertness, and gas barrier properties. DLC has thus been applied to the field of food or beverage packaging [1,2]. A technique for coating the inner surface of PET bottles with DLC has recemtly developed as a gas barrier to protect the contents, and the DLC-coated PET bottles have been commercialized for several years mainly for soft drinks in Japan [3,4]. Recently, the barrier property of inorganic thin film against potential contaminants from recycled PET was reported [5,6], and it is expected as one of effective barrier to keep contents safe.

When considering the reuse process of the bottles, they need to be washed repeatedly with alkaline solution.

Therefore, to assess whether DLC-coated PET bottles can be reusable, the effect of washing with alkaline solution on the properties of PET bottles should be investigated. Moreover, in the repeated using, pollution to the bottle itself by toxic chemicals, which is triggered by consumer misuse, is expected and it cause damage to human health. From the chemical inertness and elaborateness, DLC have a potential acting as barrier layer against these pollutions.

In this research, we evaluated the usability of DLC coating PET bottles in reuse process. For assessing the effect of washing with alkaline solution on the gas barrier property of DLC-coated PET bottles, the oxygen transmission rate was compared before and after washing. The protection of DLC coating to the chemical pollutant was assessed from gas chromatographic analysis.

2. MATERIALS AND METHODS

(1) Samples Preparation

In all experiments, standard type PET bottles used for carbonated soft drinks, 500 ml in volume and 300 μm in thickness, were used (Tomikawa Chemical Industries Co., Ltd., Japan). DLC films were coated on the inner surface of the bottles synthesizing from acetylene gas (C2H2) by a radio frequency (13.56 MHz) plasma enhanced chemical vapor deposition (RF-PECVD) method under reduced pressure using a custom-designed apparatus, details of which were described in previous paper [3]. The RF power, pressure in the chamber, gas flow rate, and coating time were 800 W, 1.0 torr, 70 sccm, and 1.8 sec, respectively. Here it should be noted that the coating process consisted of two steps; the first step was coating during the gas replacement from air to C_2H_2, and the second step was coating after completion of gas replacement. The gas replacement took 1 sec. for completion. The first step was 0.7 sec. for making gradient component region of DLC layer to improve the coating adhesiveness, and the second step was 1.1 sec. after the completion of the gas replacement for making pure dense DLC region of DLC layer. The thickness of DLC layer was measured by TEM (EM002-BF, TOPCON TECHNOHOUSE, Japan)

(2) Gas Barrier Property Analyses of Repeatedly Washed Bottles

All the bottles were soaked for 10 min at 55°C in 0.3 w/w% of sodium carbonate base washing detergent (Pancleaner SF2, Diversey Co., Ltd., Japan) whose resulting alkaline condition was approximately pH 10.7, and after detergent process, soaked in water for 10 min. at room temperature, and finally rinsed with water jetting. This procedure was repeated 15 times.

After drying of each samples in air, the oxygen transmission rate (OTR) was measured by an oxygen transmission tester (Ox-Tran 2/21 model; Mocon, Inc., USA) based on coulometric method defined by ASTM D 3985-81 [3]. The results of this measurement are expressed as the mean of 3 replicates and the corresponding standard deviation.

(3) Preparation of Polluted Bottles

As surrogate contaminants, toluene and 1,1,1-trichloroethane were

selected. Both of contaminants have volatile and are non-polar and slight-polar respectively. The contaminants were adjusted to 0.1 wt.% solutions with purified water. Each solution was introduced into the both virgin PET bottle and DLC coated PET bottle (four bottles for each bottle type and surrogates). The bottles were closed with a cap, and then they were stored in 14 days, the temperature varying 40°C. Then, the surrogate contaminant solutions were drained and the bottles were stored for 10 min at 55°C with a 0.3 wt.% solution of washing detergent (Pancleaner SF2, Diversey Co., Ltd., Japan) adjusted to pH 10.7. Residual detergent were buffered with 0.01 wt.% aqueous solution of citric acid adjusted to pH 3 at 20°C, then the bottles were rinsed with tap water and dried in air.

(4) Migration Testing to Food Simulants

For the migration tests, 4% aqueous acetic acid solution and 50% aqueous ethanol solution were used as food simulants. The polluted bottles with washing were filled with these simulants and sealed by caps, then were stored for 14 days in 50°C. After migration, 100 µl of solution was immediately extracted from bottles as the analytical samples.

The concentration of the toluene was determined with gas chromatography (GC2014, Shimadzu corp., Kyoto, Japan) equipped with a separation column, which has 3.1 m × 3.2 mm i.d. containing SBS-120 12% Shincarbon A 60-80 mesh packing material (Shinwa chemical industries ltd., Kyoto, Japan), and connected to flame ionization detector (FID-2014, Shimadzu corp., Kyoto, Japan). The concentration was quantified by internal standard method. As an internal standard solution, 10 µl of fluorobenzen dissolved in 10 ml ethanol was prepared and 300 µl of solutions added to the samples. The following GC parameters were kept constant: detector temperature, 200°C; injector temperature, 200°C; injection ode, split less; injection volume, 1 µl. The column temperature was fixed with 90°C. Nitrogen was used as carrier gas at 30 ml min^{-1}.

For determination of 1,1,1-trychroloethane, gas chromatography (6890A, Agilent technologies, USA) coupled with mass spectrometer (JMS-GCmate2, JEOL, Japan) in the selective ion mode (SIM) was used. The gas chromatographic conditions were as follows: the separation column was 25 m × 0.25 mm i.d. and 3 µm film thickness (PORABOND Q, Varian Inc., USA). Injector temperature, 250°C; injection

mode, split less; injection volume, 1 µl. Column temperature program: 50°C (3 min), from 50–300°C at 10°C/min. Carrier gas: He, at a flow rate of 1.0 ml/min. Quantification was achieved by external calibration using standard solutions of the surrogates.

(5) Quantification of Contaminants Adsorption to the Sample Bottles

The concentration of the pollutants adsorption to inner wall of bottles was analyzed by GC/FID. After washing process, the bottles were immediately cut in pieces of approximately 8 grams, then these specimens were placed in a 40-ml septum vials respectively. The vials were stored for 1 hour at 80°C and one ml of headspace were extracted, then introduced to gas chromatograph. Analyzing conditions of GC/FID was the same with setting in migration testing.

3. RESULTS AND DISCUSSIONS

(1) Bottles Appearance and DLC Film Observation

The appearances of both uncoated and DLC-coated PET bottles before and after washing (15 times of repeated washing) are shown in Figure 1. As can be seen, the DLC-coated bottle became slightly colored, which indicates that the inner wall of the bottle was successfully coated with DLC. Moreover, it can be observed that the DLC-coated bottle maintained its color even after 15 times washing, which implies the durability of DLC or its strong adhesiveness to PET bottles. Figure 2 shows the cross-sectional TEM image of DLC-coated PET substrate. From this image, the film thickness was estimated to be approximately 30 nm.

(2) Oxygen Transmission Rate Testing

Figure 3 shows the OTR for each bottle. Before washing, the OTR for DLC-coated bottles was less than one twentieth of that for uncoated bottles, which demonstrates that the gas barrier property of PET bottles was significantly improved by coating the inside surface of bottles with DLC. After 15 times of washing, the OTR for DLC-coated bottles slightly increased, indicating the deterioration in the gas barrier prop-

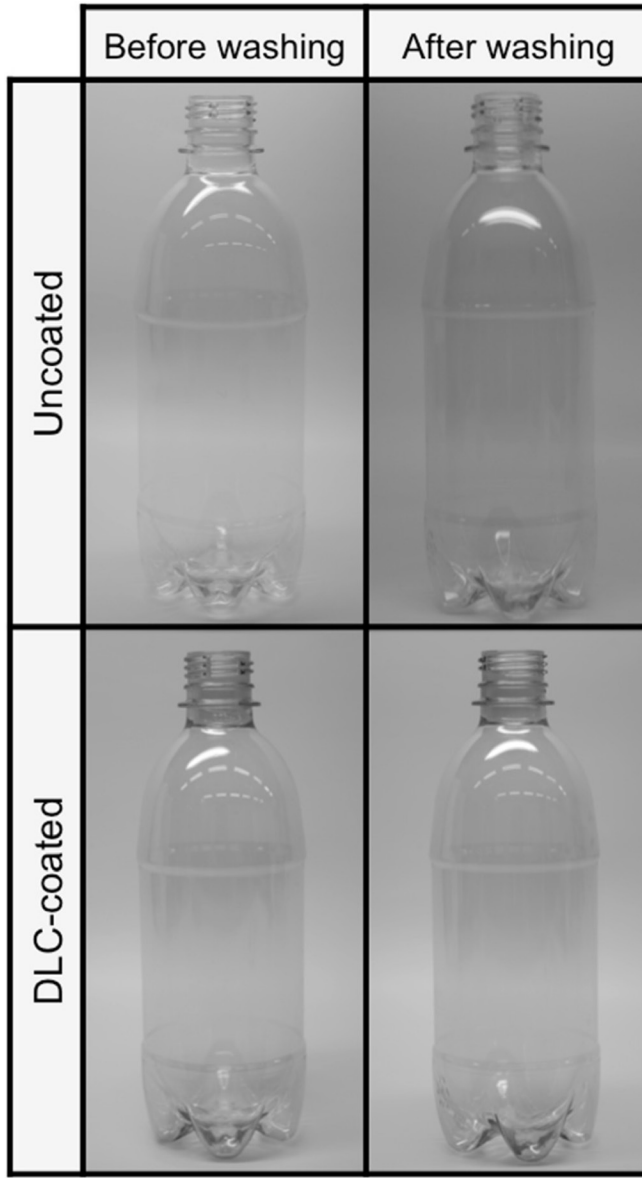

Figure 1. *Pictures of uncoated and DLC-coated PET bottles before and after washing.*

erty. However, the OTR was still much lower than that of uncoated bottles, which demonstrates that high level of oxygen barrier property of PET bottles improved by DLC coating could be maintained even after repeated washing for practical use.

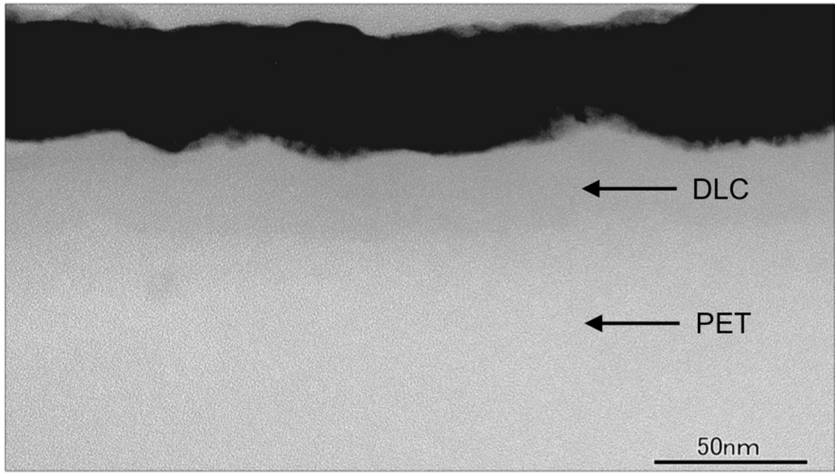

Figure 2. *TEM image of DLC-coated PET specimen.*

(3) Analyze of Migration Tests and Bottle Wall Contamination

The result of migration tests for toluene, at contact condition of two weeks at 50°C into 50% ethanol and 4% acetic acid, are given in Figure 4. It can be observed in Figure 4 that the DLC-coated bottles approximately promoted reduction of the contaminants migration to the both food simulants under one-tenth when compared with virgin PET bottles. For 1,1,1-trichloroethane, at same contact condition as that for toluene, the migration amounts from DLC-coated bottles were 0.01

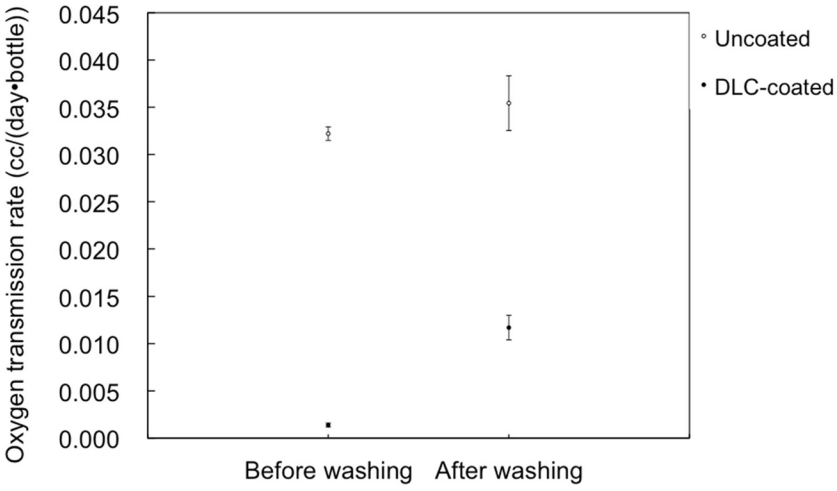

Figure 3. *Oxygen transmission rate for each bottle.*

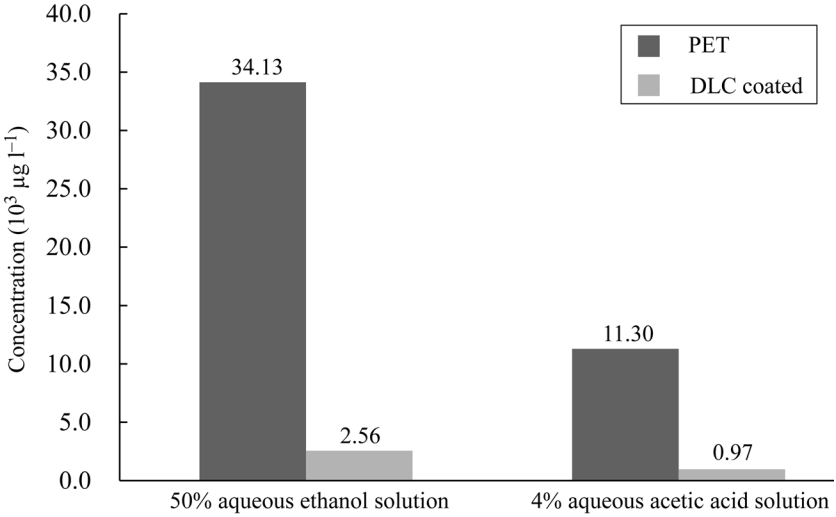

Figure 4. *Surrogate contaminants migration into 4% acetic acid over two weeks at 50°C.*

µg/l or less and also reduced compared with virgin PET bottles (Figure 5). Basically, toluene and 1,1,1-trichloroethane are used as good solvent to organic compounds and the solubility parameter of PET is close to both chemicals. In contrast, DLC is inorganic and chemically inertness. From these reasons, it is expected that the virgin PET bottles had been gradually impregnated with the chemicals in pollution process, while

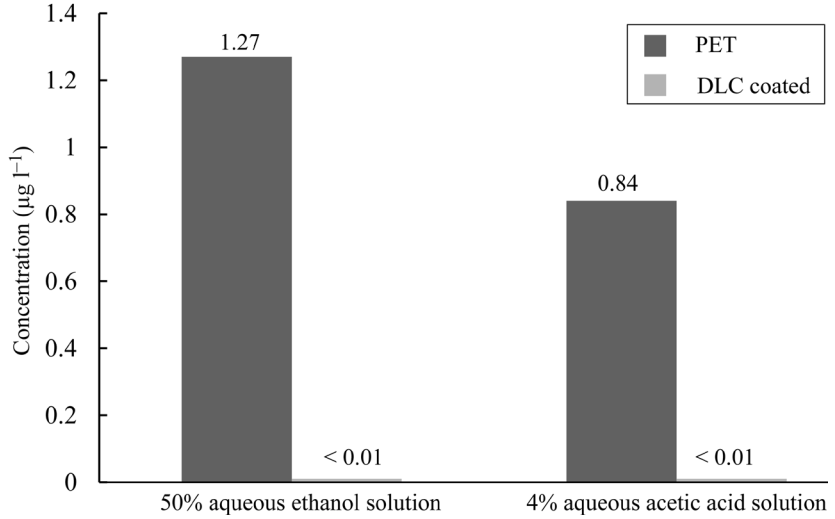

Figure 5. *Surrogate contaminants migration into 50% ethanol over two weeks at 50°C.*

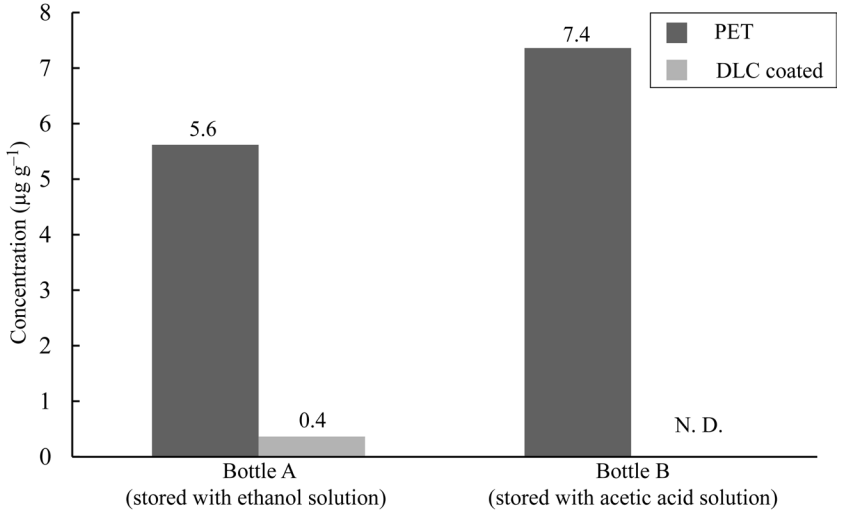

Figure 6. *Residual toluene concentration after migration tests.*

DLC-coated bottles protect the invasion of pollutants into the bottle wall. It is also suggested from contained amount of pollutant to the bottle wall. As shown in Figure 6 and Figure 7, the contaminants are detected from all of virgin PET bottles. In contrast, these are not detected from DLC-coated bottles except the case of toluene migration to the 50% aqueous ethanol solution.

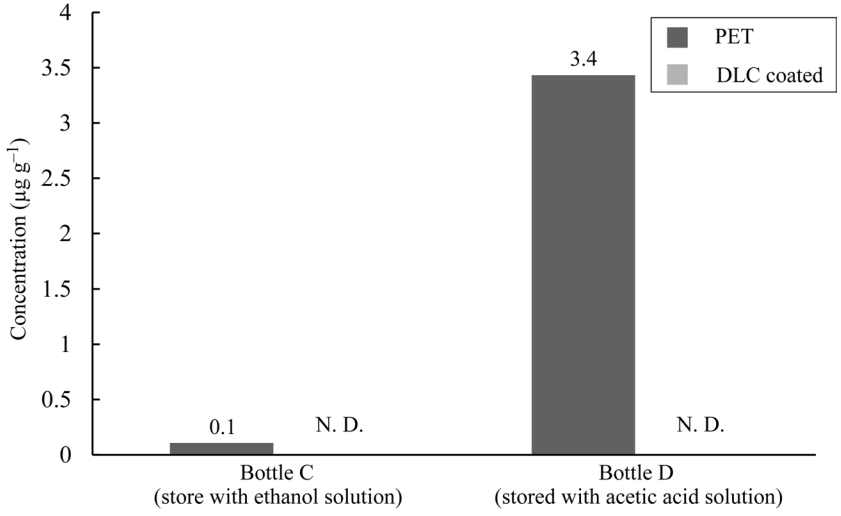

Figure 7. *Residual 1,1,1-trichroloethan concentration after migration tests.*

CONCLUSION

The results described above demonstrate that the improved gas barrier property of PET bottles due to DLC coating could be maintained even after washing with modest alkaline solution, and DLC coating bottles reduced migration of chemical pollutants into food simulants by protecting of contaminants adsorption to PET. These results indicate that DLC-coated PET bottles have potential for reuse. However, further investigation is needed to confirm the reusability of DLC-coated PET bottles. Since conventional uncoated PET bottles are likely to adsorb the constituents of the contents such as flavor compounds [7], it is essential to investigate whether DLC coating blocks adsorption or migration of such constituents. Moreover, during the reuse process, the bottles can be damaged or hydrolyzed with detergents of either alkaline or non-alkaline solution practically used for sanitarily-secured washing, which may shorten the lifetime of the bottles [8]. Therefore, we have worked on the investigation of the effect of repeated washing on such properties. The effect of the process on the quality, i.e. flavor or taste, of filling has also been analyzed.

ACKNOWLEDGEMENT

This work was supported by the Kanto Economic Affairs Bureau, Ministry of Economy, Trade and Industry, Japan.

REFERENCES

1. Finch DS, Franks J, Randall NX, Barnetson A, Crouch J, Evans AC, Ralph B., *Packaging Technology and Science. 9*(2):73–85 (1996).
2. Shimamura E, Nagashima K, Shirakura A. . Paper presented at: 10th IAPRI World Conference on Packaging; date; Melbourne, Australia (1997)
3. Shirakura A, Nakaya M, Koga Y, Kodama H, Hasebe T, Suzuki T., *Thin Solid Films* 494:84–91(2006).
4. Suzuki T, Kodama H. *Diamond and Related Materials.* 18:990–994 (2009).
5. Cruz SA, Zanin M, Nerin C, De Moraes MAB., *Food Additives and Contaminants. 23*(1):100–106 (2006).
6. Welle F, Franz R., *Food Additives and Contaminants. 25*(6):788–794 (2008).
7. Widen H, Hall G., *LWT-Food Science and Technology. 40*(1):66–72 (2007).
8. Karayannidis GP, Achilias DS., *Macromolecular Materials and Engineering. 292*(2):128–146 (2007).

The Shock Response Spectrum of the Suspension Packaging System under Rectangular Pulse

LEI WANG and AN-JUN CHEN*
School of Mechanical Engineering, Jiangnan University, 1800 Lihu Road, Wuxi, Jiangsu 214122, P.R.China

ABSTRACT: While researching the suspension-spring-style cushion packaging system, we obtained the maximum shock response spectra after established the geometric nonlinear dimensionless dynamical equations. Meanwhile, the influences on the spectra and acceleration response of dimensionless pulse peak, the angle of suspension spring and the damping ratio of system were discussed. The result shows that these kinds of influences are particularly noticeable, and that the increasing damping can effectively decrease the maximum shock response acceleration of the system. The proposed method provides references for design of shock absorber with suspension spring system.

INTRODUCTION

SUSPENSION CUSHION PACKAGING is particularly used to protect the precision instrument, such as microwave high-power tube and guide apparatus etc., which can reduce the vibration from each direction [1]. The product is suspended in the package container with spring which can reduce the vibration and shock. Studies has shown that the suspension spring system which is geometric nonlinear is superior to linear system on vibration reduction effect. Wu Xiao discussed the natural vibration and the vibration characteristics of suspension system on base displacement [2]. Xu Xiao did primary research on the vibration and shock characteristics of the suspension system, but failed to clearly propose the effects of this system's geometric nonlinearity [3]. The present studies about the suspension spring system were mostly focused on analysis of the natural vibration features and the corresponding influencing factors. And the shock characteristics were not discussed as yet.

Nonlinear packaging systems studied in packaging dynamics mostly

*Author to whom correspondence should be addressed. Email: caj62@163.com

1557-7244/11/04 237-10

referred to the nonlinearity of the cushioning material itself [4]. The analysis of the shock characteristics published was focused on the material nonlinearity [5–12].There were no discussions about the nonlinear caused by its structure.

In this article, suspension spring system was taken as the object of this study, and the dimensionless shock dynamics equation was developed under the rectangle pulse. The dynamic equations were solved by using the fourth-order Runge-Kutta method. A new concept of the three-dimensional shock response spectrum was gained. The influences to the spectrum by pulse duration, the angle of the spring and the damping were discussed. These discussions can provide theory references to the design of the suspension system.

Dimensionless Shock Equation

Descriptions of Suspension System

The suspension spring system is shown in Figure 1. A packaged product is supported by eight springs which own the same stiffness and length (four springs on the upside, and the other four springs on the downside). The dotted line describes the springs' original length. $HF_0 = GE_0 = AB_0 = DC_0 = l_0$, l_0 denotes the initial length of the spring, and $\angle GHF_0 = \angle HGE_0 = \angle DAB_0 = \angle ADC_0 = \angle ADC_0 = \varphi_0 \cdot \varphi_0$ is the angle of primary suspension position, k is the stiffness coefficient. c is the

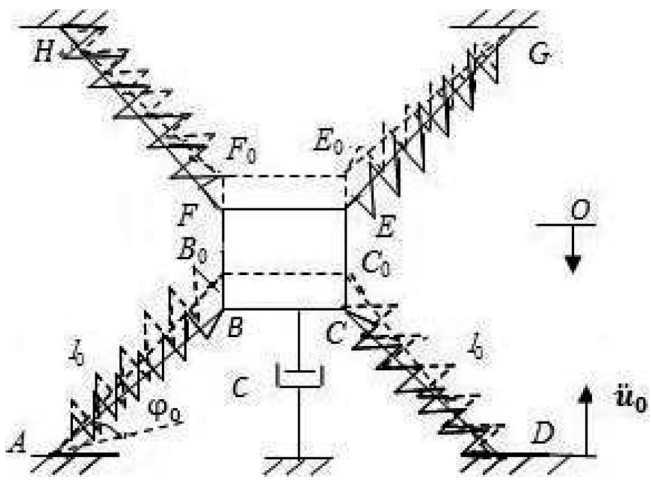

Figure 1. *The model of suspension spring system.*

equivalent damping and m is the mass of the product. $\ddot{u}_0$ is the extrinsic motivation.

Dimensionless Dynamic Equations

Supposed the packaged product dropped x_0 when the system reach the static equilibrium status. The angles of the system are then presented as $\angle DAB = \angle ADC = \varphi_1$, $\angle GHF = \angle HGE = \varphi_2$, the lengths of the springs are then written as $AB = CD = l_1$, $HF = GE = l_2$

$$l_1 = \sqrt{l_0^2 \cos^2 \varphi_0 + (l_0 \sin \varphi_0 - x_0)^2} \tag{1}$$

$$l_2 = \sqrt{l_0^2 \cos^2 \varphi_0 + (l_0 \sin \varphi_0 + x_0)^2} \tag{2}$$

The static balanced equation of the system is then written as

$$4k(l_0 - l_1)\sin \varphi_1 + 4k(l_2 - l_0)\sin \varphi_2 = mg \tag{3}$$

The coordinate system is established, with the original point taken as the static equilibrium position and the forward direction set as downward. The lengths of the springs are written as

$$l_3 = \sqrt{l_1^2 \cos^2 \varphi_1 + (l_1 \sin \varphi_1 - x)^2} \tag{4}$$

$$l_4 = \sqrt{l_2^2 \cos^2 \varphi_2 + (l_2 \sin \varphi_2 + x)^2} \tag{5}$$

A force balance in the vertical direction produces the nonlinear differential equation of motion

$$m\ddot{x} = mg - c\dot{x} - \frac{4k(l_0 - l_3)(l_1 \sin \varphi_1 - x)}{l_3} - \frac{4k(l_4 - l_0)(l_2 \sin \varphi_2 + x)}{l_4} \tag{6}$$

Substitute the Equation (4) and the Equation (5) to Equation (6), and then using Taylor series expansion and omitting the higher orders, we can obtain the approximate dynamic equation as

$$m\ddot{x} + c\dot{x} + 4k\left(a_0 x + \frac{b_0}{l_0^2} x^3\right) = 0 \tag{7}$$

Where $a_0 = 2\sin^2 \varphi_0$, $b_0 = 1 - 6\sin^2 \varphi_0 + 5\sin^4 \varphi_0$.

The base acceleration $\ddot{u}_0(t)$ is assumed as a rectangular pulse given by

$$\ddot{u}_0(t) = \begin{cases} \ddot{u}_{om} & 0 \le t \le t_0 \\ 0 & t > t_0 \end{cases} \tag{8}$$

Where t_0 is the pulse duration and $\ddot{u}_{om}$ is the pulse magnitude.

Impact dynamic equation of the system is governed by

$$m\ddot{x} + c(\dot{x} + \dot{u}_0) + 4k\left(a_0(x + u_0) + \frac{b_0}{l_0^2}(x + u_0)^3\right) = 0 \tag{9}$$

Where $x(0) = 0$ and $dx(0)/dt = 0$ are the initial displacement and velocity at the start of the shock pulse.

Letting

$$y = \frac{x + u_0}{l_0}, \quad \omega = \sqrt{\frac{4k}{m}}, \quad T = \frac{1}{\omega} \tag{10}$$

Equation (3) can be non-dimensioned as follow,

$$\frac{d^2 y}{d\tau^2} + 2\xi \frac{dy}{d\tau} + (a_0 y + b_0 y^3) = \beta \ddot{u}_{om} \tag{11}$$

Where ω is the circular frequency of the system, T is the periodic parameter, $\tau = t/T$ is the dimensionless time duration, $\tau_0 = t_0/T$ is the dimensionless pulse time, $\xi = c/4\sqrt{km}$ is the damping ratio parameter, and $\beta = T^2/l_0$ is the characteristic parameter of the system.

The initial conditions are then obtained as $y(0) = 0$ and $dy(0)/d\tau = 0$, respectively.

The non-dimensional base acceleration is then expressed as

$$\beta \ddot{u}_o = \begin{cases} \beta \ddot{u}_{om} & 0 \le \tau \le \tau_0 \\ 0 & \tau > \tau_0 \end{cases} \tag{12}$$

According to the system's shocking dynamic equations, the parameters such as the angle of the system, peak pulse acceleration and pulse

duration and damping ratio will affect the results of equations. In order to research these influences, the fourth-order-Runge-Kutta method is used to analyze characteristics of the system under the rectangular pulse.

Response of Acceleration

It can be seen from Equation (10) that

$$x'' = \frac{d^2x}{l_0 d\tau^2} = \frac{d^2y}{d\tau^2} - \frac{d^2u_0}{l_0 d\tau^2} = \frac{d^2y}{d\tau^2} - \beta\ddot{u}_{0m} \tag{13}$$

Where x'' is the dimensionless acceleration.

The response of acceleration of the system is shown in Figure 2(a) under the different angle of the suspension spring .The acceleration response of the system is shown in Figure 2(b) under the different dimensionless peak pulse acceleration. The influence of the dimensionless pulse duration on the acceleration response is shown in Figure 2(c). The acceleration response of the system with the damping is shown in Figure 2(d).

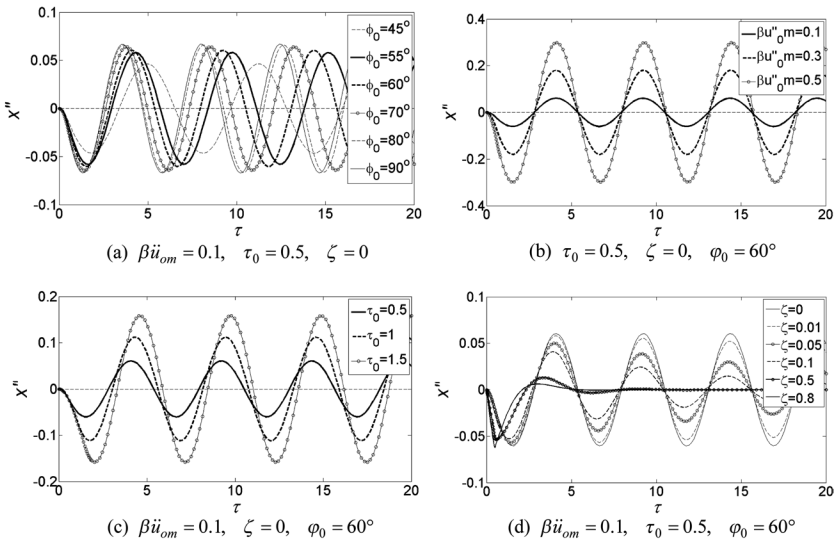

(a) $\beta\ddot{u}_{om} = 0.1, \quad \tau_0 = 0.5, \quad \zeta = 0$ (b) $\tau_0 = 0.5, \quad \zeta = 0, \quad \varphi_0 = 60°$

(c) $\beta\ddot{u}_{om} = 0.1, \quad \zeta = 0, \quad \varphi_0 = 60°$ (d) $\beta\ddot{u}_{om} = 0.1, \quad \tau_0 = 0.5, \quad \varphi_0 = 60°$

Figure 2. *The acceleration response of the system under the rectangular pulse: (a) The influence of different angle φ_0; (b) The influence of the dimensionless peak pulse acceleration $\beta\ddot{u}_{om}$; (c) The influence of dimensionless pulse duration τ_0; (d) The influence of damping ratio ζ.*

Shock Response Spectrum

According to the shock dynamic equation, the solutions are related to the angle of spring, dimensionless peak pulse acceleration, dimensionless pulse time and damping ratio. Method of fourth order Runge-Kutta was adopted to solve the dimensionless shock dynamic equation.

2D Shock Response Spectrum

The 2-dimensional shock response spectra under the rectangle pulse are obtained in Figure 3. The influence of the angle is shown in Figure 3(a). The influence of the damping is shown in Figure 3(b). According to the figure, the angle of the spring and the damping can affect the shock response spectrum.

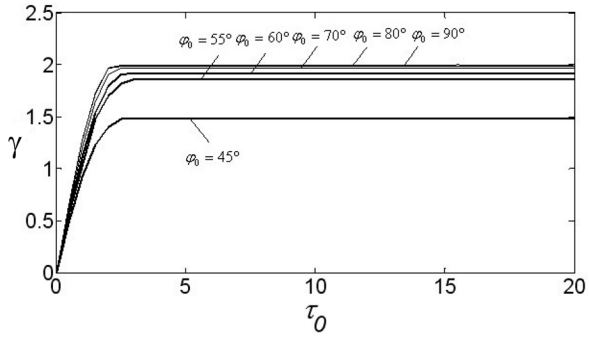

(a) $\beta\ddot{u}_{om} = 0.3$

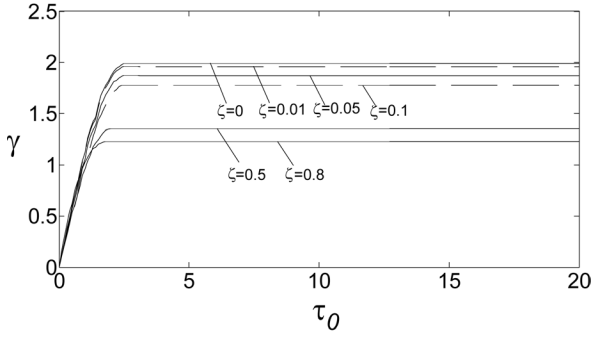

(b) $\beta\ddot{u}_{om} = 0.1, \quad \varphi_0 = 60°$

Figure 3. *2D shock response spectrum under the rectangle pulse: (a)The effect of the different angle; (b)The effect of the damping.*

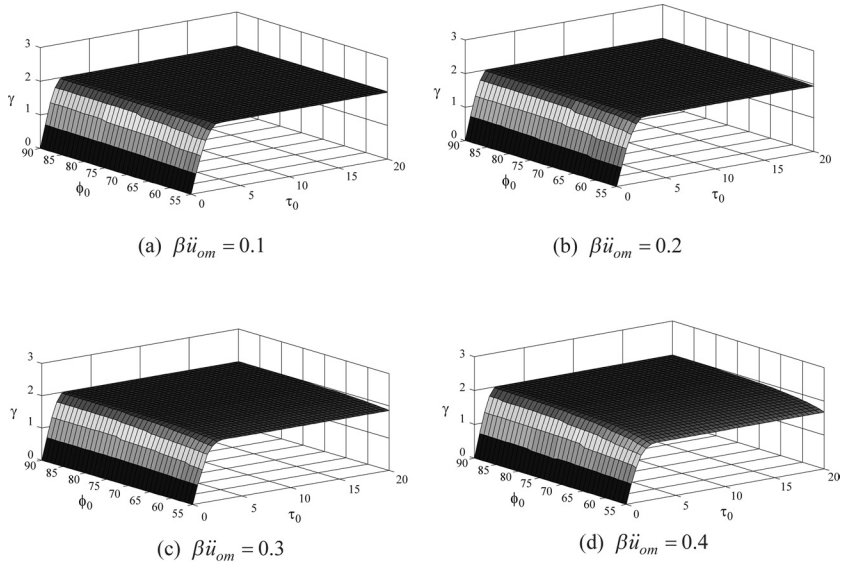

Figure 4. *Shock response spectra of suspension spring system under the rectangle pulse without damping*

3D Shock Response Spectrum

According to the structure of the suspension system, a new concept of 3-dimensional shock response spectrum is established. The ratio of the maximum shock response acceleration of the system to the peak pulse acceleration $\gamma = (\ddot{x})_m / \ddot{u}_{0m}$, the pulse duration τ_0 and the angle of the system's suspension spring φ_0 are selected as basic evaluation quantities for the three-dimensional shock response spectra under the rectangular pulse. The angle of the suspension spring ranges from 55° to 90° and the dimensionless pulse duration is limited from 0 to 20. The dimensionless peak pulse acceleration is taken as 0.1, 0.2, 0.3 and 0.4. The influences of the shock response spectrum without damping are shown in Figure 4. Figure 5 shows the influences of the shock response spectrum with damping, whose actual values range from 0 and 1, and for the convenience research, which are taken as 0.01, 0.1, 0.5 and 0.8 as an example.

Proof of the Numerical Method

The numerical method is adopted to solve the response of the system. The correctness of the numerical method need to be proved. Thus,

the special value method is chosen to prove the numerical method. The system is a linear system when the angle $\varphi_0 = 90°$, the response of the special case under the rectangle pulse is calculated with Runge-Kutta method. The analytic solution of the linear system is also calculated. The data are shown in Table 1. Comparing the data, the relative error is very small. So the numerical method used in the paper is appropriate for the nonlinear system.

CONCLUSIONS

In this article, the shock spectra for suspension system are developed. Figures 2 through 5 show that the peak amplitude is no more than 2 times of pulse incentive amplitude under the rectangle pulse. According to the figures, pulse duration, the angle of the spring and the damping can affect the shock characteristics of the suspension spring system. There were several influences as follows:

1. According to Figure 2, the vibration effect of the suspension system is superior to linear system ($\varphi_0 = 90°$) without the damping. The period of acceleration response of the suspension system is extended, the frequency and the amplitude of acceleration re-

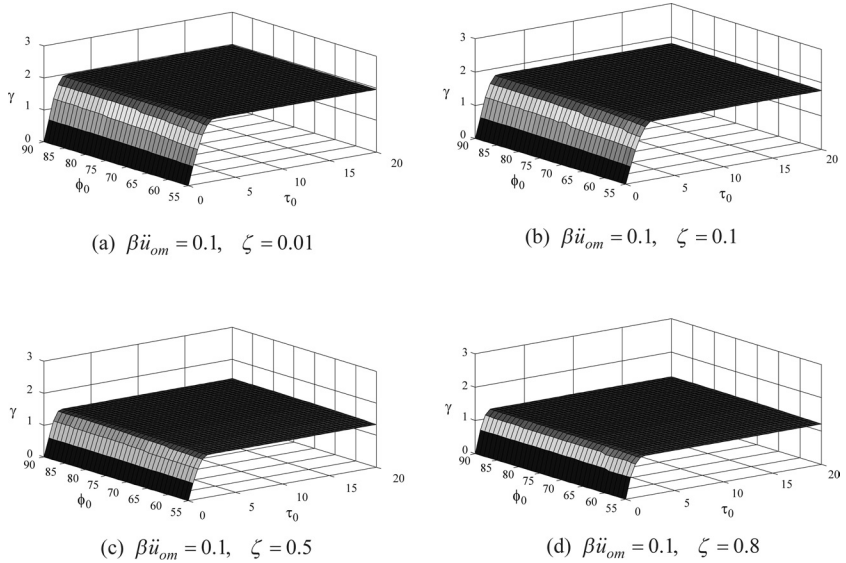

Figure 5. *Shock response spectra of suspension spring system under the rectangle pulse with damping.*

Table 1 Comparison Numerical Method with Analytic Solution..

τ_0	**0.628**	**1.256**	**1.884**	**2.512**	**3.14**	**6.28**	**31.4**	**62.8**
Analytic Solution	0.6180	1.1756	1.6180	1.9021	2	2	2	2
Numerical Method	0.6151	1.1860	1.5985	1.9024	1.999	2	2	2
Relative Error	0.47%	0.88%	1.21%	0.02%	0.05%	0	0	0

sponse decreases as the angle of the spring let up under the given conditions.Therefore, the designer can adjust the angle properly to reduce the damage of the product. The acceleration response amplitude increased as the dimensionless pulse amplitude and pulse duration added. The amplitude of the response can decrease when the damping increased. The packaged product can get the best buffing effect by considering these factors synthetically.

2. The response amplitude of system increases rapidly to the peak value and then reaches the steady status under the rectangle pulse. The peak value will not change along with the pulse duration any more. $\beta\ddot{u}_{om} = (T^2/l_0)\ddot{u}_{0m}$, $\ddot{u}_{0m}$ is affected by the environment. The effect of the dimensionless shock amplitude can be decreased by increasing the length of the spring in the design of the system.
3. Comparing to the linear system, the system response decreases clearly when the angle of system reduces under a certain system damping and pulse duration. The response amplitude reduces evidently when the angle is less than 75°. According to the Equation (7), the system have soft-spring characteristic when the suspension angle φ_0 ranges from 55° to 90°.The system can achieve good impact effect as long as enough stiffness.
4. The amplitude of response was affected rapidly by damping. The response amplitude can significantly decrease when damping increases and this effect is more obvious when pulse incentive amplitude adds. According to this feature, the buffer performance of the package can be optimized. According to the study, these rules can provide the basis for the packaging optimized design.

REFERENCES

1. G.X. Peng.1999. *Printing Industry Publishing House: Transportation Packaging,* Beijing. (In Chinese).
2. X.Wu and L.J.Yang,Natural Vibration Property of Geometrically Nonlinear Vibration Isolation System with Suspension Springs, *Journal of Vibration and Shock,* Vol. 27, No. 11, 2008, pp.71–72. (In Chinese)

3. X. Xu, Analysis and Study on Suspension System with Package Cushioning, Xi'an University of Technology, 2005. (In Chinese)
4. Y.Sun and M.H.Zhang, The Non-linear Problem in the Packaging Dynamics, *Packaging Engineering,* Vol. 16, No. 1, 1995, pp. 5–10. (In Chinese)
5. Z.W. Wang, C.Y. Hu, Shock Spectra and Damage Boundary Curves for Non-linear Package Cushioning System, *Packaging Technology and Science.,* Vol. 12, 1999, pp. 207–217.
6. J.Wang, Theoretical Study on Product Damage Evaluation and Protective Packaging Dynamics, Jiangnan University, 2009. (In Chinese)
7. 7. J.Wang, Z.W. Wang,L.X.Lu.Three-dimensional Shock Spectrum of Critical Component for Nonlinear Packaging System, *Shock and Vibration,* Vol. 18, 2011, pp. 437–445.
8. Z.W. Wang, On Evaluation of Product Dropping Damage, *Packaging Technology and Science,* Vol. 15, No. 3, 2002, pp. 115–120.
9. J.Wang and Z.W.Wang, 3-Dimensional shock response spectra characterizing shock response of a tangent packaging system with critical component. *Journal of Vibration and Shock,* Vol. 27, 2008, pp. 167–173.
10. Z.W. Wang, Dropping Damage Boundary Curves for Cubic and Tangent Package Cushioning Systems, *Packaging Technology and Science,* Vol. 15, 2002, pp. 263–266.
11. G.J. Burgess, Product Fragility and Damage Boundary Theory, *Packaging Technology and Science* Vol. 15, No. 10, 1988, pp. 5–10.
12. J.Wang, L.X.Lu, Z.W.Wang.Dynamics of Product-Transport-System by Improved Inverse Sub-structuring Method, *Journal of Applied Packaging Research,* Vol. 4, No. 4, pp. 241–253, 2010.

Application of RFID Technologies to Evaluate the Packaging Insulation Performance in Pharmaceutical Supply Chain

CHANGFENG GE[1,*], DANIEL JOHNSON[1], EDMUND CHAN[2] and DEREK ANG[2]

[1]*Rochester Institute of Technology,78 Lomb Memorial Drive, Rochester, NY 144623,USA*

[2]*Republic Polytechnic, 9 Woodlands Ave 9, Singapore 738964*

ABSTRACT: A conventional temperature recorder is commonly used as a tool to monitor the temperature inside and outside of packaging to evaluate insulation properties. In recent years, radio frequency identification (RFID) technologies have integrated the temperature sensor into the RFID tag to track temperature changes in supply chain. This study used a conventional temperature sensor and RFID incorporated temperature sensors to conduct a field measurement of temperature for thermal insulation box packaging. The readability of the RFID temperature sensor and insulation performance of the packaging boxes were also investigated in the study.

1. INTRODUCTION

WITH its ability to read multiple products, cartons and totes at the same time, RFID technologies are increasingly adopted to improve logistics processes. Besides adopting RFID to enhance supply chain velocity, some high-value pharmaceutical and perishable products require close temperature monitoring as well. If the cold chain of a product is not maintained within stipulated temperature ranges, product efficacy is affected. Deterioration of pharmaceutical products can be detrimental to patient health and even safety. RFID tags incorporating temperature sensors have been developed to support the need for logistics process efficiency and temperature monitoring.

The primary objective of the study is to compare the performance of RFID temperature tags with conventional temperature recorders in

*Author to whom correspondence should be addressed. Email: awl85726@126.com

1557-7244/11/04 247-07

temperature recording for pharmaceutical products distribution. In addition, the project will investigate the effectiveness of the packaging insulation box during the field trip in a demanding summer distribution environment. The ease of retrieving temperature records from an RFID incorporated temperature sensor and conventional temperature sensors are also discussed.

2. EXPERIMENTAL DESIGN

Packaging to be Evaluated

The shipping system for the pharmaceutical product to be evaluated is described in the following figure. It consists of a corrugated board box with FEFCO code 0201 laminated with metattilzed PET film, an insulation expended polystyrene (EPS) foam with a thickness of 40mm, a divider with a space thickness of 10mm laminated metallized film for containing Phase Changing Material (PCM). The external dimension of the packaging is 485 × 390 × 388 mm. The EPS foam material has a thermal conductivity of 0.025 W/m°C. This is a common configuration used to maintain pharmaceutical products like temperature-sensitive drugs, vaccines and samples. PCM comes in different temperature maintenance ranges, and differs in by conditioning required. Multiple configurations of PCM's are used to maintain products that require varying temperature ranges for a variety of durations.

Temperature Sensors

The conventional sensor used is TempTale 4 Ambient Temperature Monitor with a measuring range of –30°C to +70°C (–22°F to +158°F) manufactured by Sensitech, USA. The RFID tag used is ThermAssureRF with a temperature range of –80°C to 150°C (–120°F to 312°F), 0 to 100% RH. produced by Evidencia LLP. As shown in the figure, the internal ThermAssureRF was placed between the products in the container; while the other ThermassureRF was placed outside of the shipping container to record the ambient temperature. The conventional sensor Temp tale 4 was placed on the top of pharmaceutical package.

Phase Changing Materials

A total 10 pieces of phase changing materials were placed in the

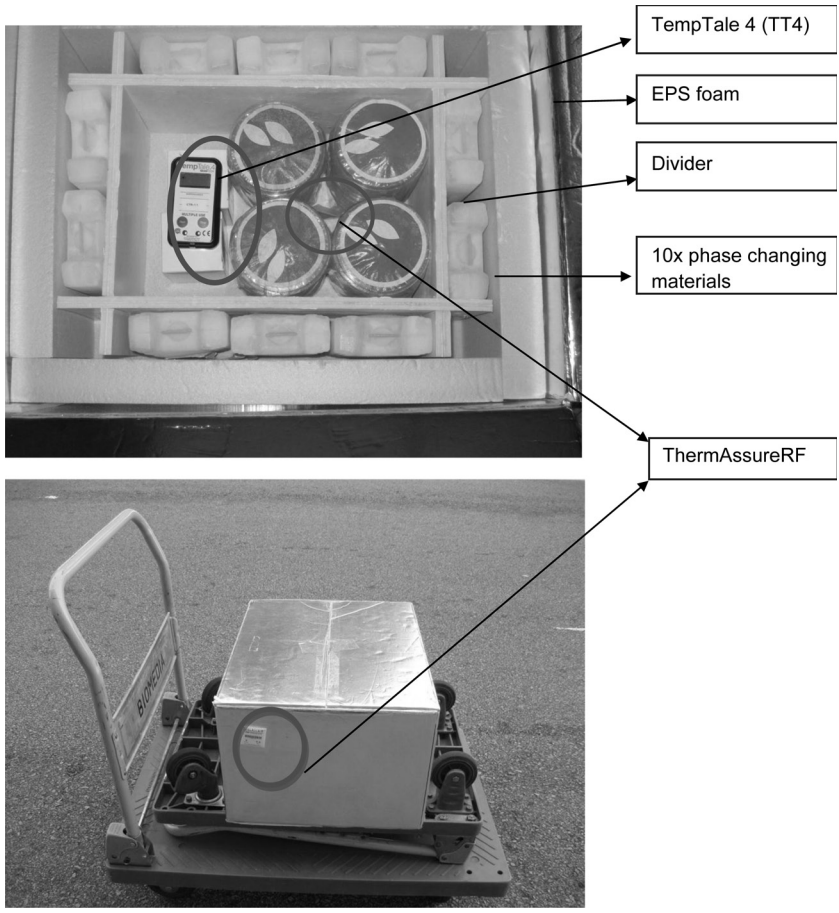

Figure 1. *Packaging insulation box and the location of the sensors*

shipping container. The phase changing material is manufactured by Emball'iso. It had to be frozen at a temperature of –18°C for at least 48 hours before it was placed in the packaging. It experiences a phase change from solid to liquid at the temperature of about +1°C.

Measurement in Distribution Channel

The pharmaceutical products were distributed with a non-refrigeration van which made multiple stops. The field measurement starts at 8:30 A.M. and ends at 5:00 P.M. on the same day. The ambient environment was approximately 32°C with a relative humidity of 98% RH, which is typical for a tropical environment. A total of 529 temperature

data points for each sensor was collected during the eight and half hour journal. Three sets of temperature data were summarized in Figure 3. They are ambient temperature recorded by RFID sensor ThermAssureRF (Evidencia LLP), the temperature around the product inside of the package recorded by RFID sensor ThermAssureRF(Evidencia LLP) and the conventional temperature sensor TempTale 4 (Sensitech) respectively.

3. ANALYSIS

Based on the captured data, thermal equilibrium, correlation between data captured by RFID sensor and conventional sensor and insulating performance of the packaging are analyzed.

Thermal Equilibrium in the Package

Shown in Figure 3, the conventional sensor (Sensitech) demonstrated a sharper drop from the ambient temperature to zero versus the RFID sensor. This is likely related to the Sensitech sensor being exposed to an open space in the package near the phase change material with an

Figure 2. *The Truck for distribution the pharmaceutical product.*

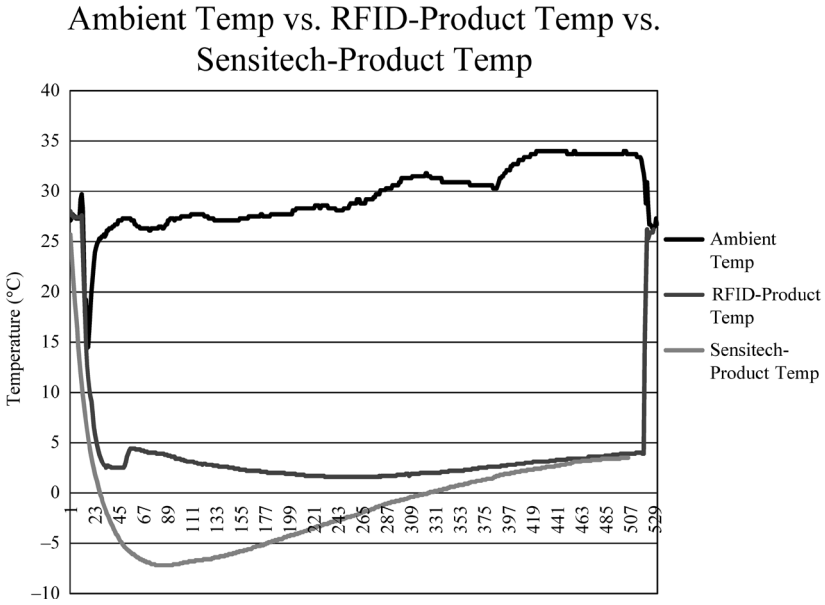

Figure 3. *Ambient, RFID sensor and conventional sensor temperature in °C.*

initial temperature of –18°C. The RFID tag was placed between the products, thus more closely reflecting the temperature change profile of the product.

Temperatures recorded by the RFID and conventional sensors demonstrated a low temperature valley before gradually reaching a temperature of 4°C. This demonstrates the "zeroth law" of thermodynamics that if two systems (product and phase changing material) are at the same time in thermal equilibrium with a third system (the container), they are in thermal equilibrium with each other. Heat flow in the package representing the heat energy from the place to place moving towards thermal equilibrium.

Pearson Correlation and t-test

Pearson correlation and an unpaired *t*-test was done at thermal equilibrium from data points 463 to 507 so as to compare the temperature measured by the RFID sensor versus conventional sensors. The correlation factor between the two group was 0.91 and the unpaired t-test yields a p value of < 0.001. This shows that there is negligible difference in the temperature taken by RFID sensor compared to conventional sensor.

Readability of the RFID Tag

The RFID temperature sensor placed outside of the box recorded the data in the entire journey and data were retrieved successfully even in a high humidity environment. The RFID reader was unable to retrieve RFID data recorded by the RFID temperature sensor between the products when the box was closed (at a distance). Though RFID tag has a capacity of capturing 6000 temperature data points, the shipping system needs to be placed very close to the reader for temperature data to be retrieved and checked for temperature violations. The RFID tag and its complementary reader used in this project has a high operating frequency range, which means that reads can be performed even through the typically wet media required by cold chain logistics.

Packaging Insulation

It was observed that the phase changing material did not have any change in weight or shape when the package was reopened upon return from distribution. Apparently the restriction of heat flow within the shipping container was adequate to keep the temperature within the box below 4°C as required. The packaging box demonstrated an excellent insulation property.

4. CONCLUSION

The study showed that the RFID temperature sensor with high frequency system was effective in measuring the temperature in a wet ambient environment of 98% RH. However, the reading distance was still limited to within 2 cm despite of the advantage being small and foldable. It would be interesting to develop an ultra high frequency (UHF) system with a similar temperature logging capability to enhance readability. At the same time the readability in wet environment is not compromised. Future work can also include installing antennas as signal boosters to improve readability over longer distances under a wet environment.

The design of insulation and phase changing material are adequate in this application. Thermal equilibrium is reached within the container. Future work could involve optimizing wall thickness of the packaging box in order to create a more cost effective sustainable packaging solution.

ACKNOWLEDGEMENT

The authors wish to thank SPD Scientific Pte Ltd in Singapore for their support to carry out the temperature recording trial base on their actual operation requirements.

REFERENCES

1. Cecilia Amador, Jean-Pierre Emond, Maria Cecilia do Nascimento Nunes, Application of RFID technologies in the temperature mapping of the pineapple supply chain, Sens & Instrument. *Food Quality,* (2009) 3:26–33.
2. Rosie Sher, "Unpaired t-tests", Loughborough University, Mathematics Learning Support Centre, (2004) Available: http://mlsc.lboro.ac.uk/resources/statistics/Unpairedttest.pdf

Guide to Authors

1. Manuscripts shall be sent electronically to the editors, Changfeng Ge at cfgmet@rit.edu and Bruce Welt at bwelt@ufl.edu using Microsoft Word in an IBM/PC format. If electronic submission is not possible, three paper copies of double-spaced manuscripts may be sent to Changfeng Ge, Editor of the *Journal of Applied Packaging Research*, Rochester Institute of Technology, One Memorial Drive, Rochester, NY 14623-5603, USA (Telephone 585-475-5391) or Bruce Welt, Editor of the *Journal of Applied Packaging Research*, University of Florida, Box 110570, Gainesville, FL 32611-0570, USA (Telephone 352-392-1864, X-111). Manuscripts should normally be limited to the space equivalent of 6,000 words. The editor may waive this requirement in special occasions. As a guideline, each page of a double-spaced manuscript contains about 300 words. Include on the title page the names, affiliations, and addresses of all the authors, and identify one author as the corresponding author. Because communication between the editor and the authors will be electronic, the email address of the corresponding author is required. Papers under review, accepted for publication, or published elsewhere in journals are normally not accepted for publication in the *Journal of Applied Packaging Research*. Papers published as proceedings of conferences are welcomed.
2. Article titles should be brief, followed by the author's name(s), affiliation, address, country, and postal code (zip) of author(s). Indicate to whom correspondence and proofs should be sent, including telephone and fax numbers and e-mail address.
3. Include a 100-word abstract and keywords.
4. If electronic art files are not supplied, submit three copies of camera-ready drawings and glossy photographs. Drawings should be uniformly sized, if possible, planned for 50% reduction. Art that is sent electronically should be saved in either a .tif or .JPEG files for superior reproduction. All illustrations of any kind must be numbered and mentioned in the text. Captions for illustrations should all be typed on a separate sheet(s) and should be understandable without reference to the text.
5. DEStech uses a numbered reference system consisting of two elements: a numbered list of all references and (in the text itself) numbers in brackets that correspond to the list. At the end of your article, please supply a numbered list of all references (books, journals, web sites etc.). References on the list should be in the form given below. In the text write the number in brackets corresponding to the reference on the list. Place the number in brackets inside the final period of the sentence cited by the reference. Here is an example [2].

   Journal: 1. Halpin, J. C., "article title", *J. Cellular Plastics,* Vol. 3, No. 2, 1997, pp. 432–435.
   Book: 2. Kececioglu, D. B. and F.-B. Sun. 2002. *Burn-In Testing: Its Quantification and Optimization,* Lancaster, PA: DEStech Publications, Inc.

6. Tables. Number consecutively and insert closest to where first mentioned in text or type on a numbered, separate page. Please use Arabic numerals and supply a heading. Column headings should be explanatory and carry units. (See example at right.)

Table 5. Comparison of state-of-the-art matrix resins with VPSP/BMI copolymers.

Resin System	Core Temp. (DSC peak)	Char Yield, %
Epoxy (MY720)	235	30
C379: H795 = 14	285	53

7. Units & Abbreviations. SI units should be used. English units or other equivalents should appear in parentheses if necessary.
8. Symbols. A list of symbols used and their meanings should be included.
9. Page proofs. Authors will receive page proofs by E-mail. Proof pages will be in a .PDF file, which can be read by Acrobat Reader. Corrections on proof pages should be limited to the correction of errors. Authors should print out pages that require corrections and mark the corrections on the printed pages. Pages with corrections should be returned by FAX (717-509-6100) or mail to the publisher (DEStech Publications, Inc., 439 North Duke Street, Lancaster, PA 17602, USA). If authors cannot handle proofs in a .PDF file format, please notify the editors, Changfeng Ge at cfgmet@rit.edu or Bruce Welt at bwelt@ufl.edu.
10. Index terms.With proof pages authors will receive a form for listing key words that will appear in the index. Please fill out this form with index terms and return it.
11. Copyright Information. All original journal articles are copyrighted in the name of DEStech Publications, Inc. All original articles accepted for publication must be accompanied by a signed copyright transfer agreement available from the journal editor. Previously copyrighted material used in an article can be published with the *written* permission of the copyright holder (see #14 below).
12. Headings. Your article should be structured with unnumbered headings. Normally two headings are used as follows:

    Main Subhead: DESIGN OF A MICROWAVE INSTALLATION
    Secondary Subhead: Principle of the Design Method

13. If further subordination is required, please limit to no more than one (*Third Subhead*).
14. Equations. Number equations with Arabic numbers enclosed in parentheses at the right-hand margin. Type superscripts and subscripts clearly above or below the baseline, or mark them with a caret. Be sure that all symbols, letters, and numbers are distinguishable (e.g., "oh" or zero, one or lowercase "el," "vee" or Greek nu).
15. Permissions. The author of a paper is responsible for obtaining releases for the use of copyrighted figures, tables, or excerpts longer than 200 words used in his/her paper. Copyright releases are permissions to reprint previously copyrighted material. Releases must be obtained from the copyright holder, which is usually a publisher. Forms for copyright release will be sent by the editor to authors on request.

General: The *Journal of Applied Packaging Research* and DEStech Publications, Inc. are not responsible for the views expressed by individual contributors in articles published in the journal.